Materials Today Bio 25 (2024) 100956

Contents lists available at ScienceDirect

Materials Today Bio

journal homepage: www.journals.elsevier.com/materials-today-bio

# Capturing cerium ions via hydrogel microspheres promotes vascularization for bone regeneration

Junlin Liu [a,b,1], Zhangzhe Zhou [a,b,1], Mingzhuang Hou [a,b,1], Xiaowei Xia [a,b], Yang Liu [a,b], Zhijian Zhao [a,b], Yubin Wu [a,b], Yaoge Deng [a,b], Yijian Zhang [a,b], Fan He [a,b,**], Yong Xu [a,b,***], Xuesong Zhu [a,b,*]

[a] Department of Orthopaedics, The First Affiliated Hospital of Soochow University, Soochow University, Suzhou 215006, China
[b] Orthopaedic Institute, Medical College, Soochow University, Suzhou 215007, China

ARTICLE INFO

*Keywords:*
Cerium ions
Microfluidic
Hydrogel microspheres
Angiogenesis
Bone regeneration

ABSTRACT

The rational design of multifunctional biomaterials with hierarchical porous structure and on-demand biological activity is of great consequence for bone tissue engineering (BTE) in the contemporary world. The advanced combination of trace element cerium ions ($Ce^{3+}$) with bone repair materials makes the composite material capable of promoting angiogenesis and enhancing osteoblast activity. Herein, a living and phosphorylated injectable porous hydrogel microsphere (P-GelMA-Ce@BMSCs) is constructed by microfluidic technology and coordination reaction with metal ion ligands while loaded with exogenous BMSCs. Exogenous stem cells can adhere to and proliferate on hydrogel microspheres, thus promoting cell-extracellular matrix (ECM) and cell-cell interactions. The active ingredient $Ce^{3+}$ promotes the proliferation, osteogenic differentiation of rat BMSCs, and angiogenesis of endotheliocytes by promoting mineral deposition, osteogenic gene expression, and VEGF secretion. The enhancement of osteogenesis and improvement of angiogenesis of the P-GelMA-Ce scaffold is mainly associated with the activation of the Wnt/β-catenin pathway. This study could provide novel and meaningful insights for treating bone defects with biofunctional materials on the basis of metal ions.

## 1. Introduction

With the advancement of the socio-economic landscape and the increasing prevalence of an aging population, critical-sized bone defects, resulting from various etiologies including diseases (e.g., osteoporosis, infections, and bone tumors) and traumatic incidents (e.g., automobile accidents and injuries), have become progressively widespread, profoundly impacting the quality of life of affected individuals [1,2]. The successful repair of critical-sized bone defects necessitates the simultaneous orchestration of angiogenesis and osteogenic differentiation, with angiogenesis serving as a prerequisite for the latter [3,4]. Currently, autologous bone transplantation with vascular pedicle remains the established clinical standard for bone repair. Nevertheless, this surgical procedure is associated with several limitations, including restricted availability, substantial surgical trauma, exacting surgical prerequisites, and suboptimal vascular integration [5,6]. One of the primary challenges in the field of bone tissue engineering revolves around the need to develop a functional vascular network by promoting angiogenesis. This is crucial to enable the efficient transportation of oxygen and nutrients to cells located at the site of the bone defect. Presently, strategies for inducing angiogenesis in bone tissue engineering predominantly encompass stem cell therapy, growth factor therapy, and gene therapy, which are characterized by either high costs or concerns regarding potential tumorigenesis [7–9]. Conventionally, angiogenesis in the context of bone tissue engineering has been induced and regulated by administering growth factors or cytokines. The vascular endothelial growth factor (VEGF), fibroblast growth factors (FGFs), and platelet-derived growth factor (PDGF) are the three types of growth factors that have been used to activate angiogenesis the most frequently and effectively [10]. However, despite the promising outcomes achieved with the

* Corresponding author. Department of Orthopaedics, The First Affiliated Hospital of Soochow University, Soochow University, Suzhou 215006, China.
** Corresponding author. Department of Orthopaedics, The First Affiliated Hospital of Soochow University, Soochow University, Suzhou 215006, China.
*** Corresponding author. Department of Orthopaedics, The First Affiliated Hospital of Soochow University, Soochow University, Suzhou 215006, China.
*E-mail addresses:* fanhe@suda.edu.cn (F. He), yxu1615@suda.edu.cn (Y. Xu), zhuxs@suda.edu.cn (X. Zhu).
[1] Junlin Liu, Zhangzhe Zhou and Mingzhuang Hou contributed equally to this work.

https://doi.org/10.1016/j.mtbio.2024.100956
Received 27 October 2023; Received in revised form 27 December 2023; Accepted 15 January 2024
Available online 24 January 2024

utilization of these biomolecules, they also exhibit certain drawbacks, such as limited stability, adverse effects, and elevated costs [11,12]. Moreover, these biomolecules are highly susceptible to degradation when exposed extracorporeally, particularly when incorporated into scaffolds [13,14]. Consequently, there is an exigent necessity for identifying more efficacious strategies in bone tissue engineering.

In this context, various alternative approaches have been explored, focusing on utilizing bioactive ions. Metal ions, specifically, demonstrate unique therapeutic characteristics such as redox activity, Lewis acidity, valence, and magnetic properties. Significantly, metal ions, when utilized as therapeutic agents, do not provide the potential for breakdown or instability [15–17]. These ions possess the ability to engage in interactions with macromolecules, such as enzymes and nucleic acids, or activate ion channels, so exerting an influence on biological processes [18–20]. Moreover, metal ions have an exceptional capacity to preserve their stability during the production of biomaterials, especially in situations that involve the utilization of organic solvents or elevated temperatures. Utilizing metal ions for tissue regeneration offers several notable advantages compared to protein growth factors. These advantages include cost reduction, elimination of decomposition concerns, improved stability, and increased efficacy even at lower concentrations [21]. Currently, the range of metal ions utilized in the field of tissue engineering includes cobalt, copper, calcium, chromium, gallium, iron, lithium, magnesium, manganese, silver, strontium, vanadium, and zinc. Notably, most of these ions play a crucial role as cofactors for enzymes [17,22]. Additionally, small quantities of rare earth elements, such as lanthanum (La), cerium (Ce), and gadolinium (Gd), are naturally present in the human body, participating in processes related to stem cell differentiation and tissue regeneration. Studies have indicated relatively high cerium deposits in human bones, suggesting that bones may serve as the primary site for cerium accumulation [23–26]. In comparison to $Ca^{2+}$ (with an ionic radius of 1.06 Å), cerium ions closely approximate the size of calcium ions, with $Ce^{3+}$ measuring at 1.04 Å and $Ce^{4+}$ at 0.97 Å [27]. Cerium ions have been shown to stimulate the proliferation, differentiation, and mineralization of osteoblasts, increase collagen production in human mesenchymal cells, and enhance the mechanical properties of bones, although the precise mechanisms involved remain to be elucidated [28]. Consequently, the use of metal ion-loaded biomaterials as potent carriers for controlled release of specific therapeutic ions represents a highly promising strategy in the field of bone tissue engineering.

Hydrogel microspheres with diameters ranging from 1 μm to 1000 μm have emerged as advanced functional materials within the field of biological applications. The microspheres resemble the native extracellular matrix (ECM), making them well-suited for a range of applications such as drug administration, tissue engineering, biosensing, and cellular life science investigations [29,30]. By providing a larger specific surface area, hydrogel microspheres serve as carriers for cell delivery, facilitating the exchange of oxygen and nutrients between cells and the extracellular microenvironment. This, in turn, fosters enhanced interactions among cells and the ECM, as well as intercellular interactions, ultimately amplifying the cellular paracrine effect [31]. The successful utilization of microspheres in these diverse applications hinges on their unique characteristics, encompassing size, structure, composition, and configuration. Hence, the controlled fabrication of microspheres is imperative to enhance their reliability in the context of biological research [32–34]. The utilization of droplet microfluidics has emerged as a very suitable method for producing microparticles with uniform size, shape, and desired properties, enabling efficient and accurate control over these characteristics in a large-scale production process. Moreover, with exceptional efficacy, it facilitates the on-chip encapsulation of various bioactive substances, such as pharmaceuticals, cells, and other biological reagents. Furthermore, it facilitates the simultaneous encapsulation of numerous components. The manipulation of particle size, structure, and composition allows for the attainment of improved retention and regulated release of bioactive compounds [35,36]. Thus, hydrogel microspheres stand as a promising carrier in addressing critical-size bone defects.

In this study, P-GelMA-Ce composite microspheres were successfully fabricated through microfluidic technology and non-covalent coordination chelation reactions. These microspheres exhibit controlled and gradual release of cerium ions, which in turn facilitate adhesion, proliferation, angiogenesis, and osteoblast differentiation, ultimately promoting the healing of critical-size bone defects. The fabrication process involved the grafting of polyphosphate onto the GelMA skeleton, followed by the preparation of highly uniform photocrosslinked P-GelMA microspheres using the microfluidic method. Subsequently, $Ce^{3+}$-capturing P-GelMA-Ce@BMSCs composite microspheres were developed by simultaneously incorporating exogenous BMSCs through metal ion coordination ligands (Scheme 1). In vitro cell experiments were used to verify the characteristics of composite microspheres, including cell biocompatibility, cell proliferation potential, and the ability to promote blood vessel formation and bone formation. To validate the ability of the composite microspheres in promoting bone regeneration, the rat model featuring critical-size bone defects was comprehensively evaluated using Micro-CT and tissue section staining. In summary, this study presents the development of a living, phosphorylated, and injectable hydrogel microsphere that releases $Ce^{3+}$ to modulate the bone regeneration microenvironment, thereby enhancing bone repair.

## 2. Material and methods

### 2.1. Materials

Gelatin Methacryloyl (GelMA, EFL-GM-30) was purchased from EFL Technology Company (Suzhou, China). Imidazole, EDC-HCL, sodium hexametaphosphate, sodium hydroxide (NaOH) anhydrous cerium chloride, alcohol, and 3 % $H_2O_2$ are provided by Sigma Aldrich. Isopropyl myristate and dehydrated sorbitol oleate (Span 80) were purchased from Macklin Biochemical Technology Co., Ltd. (Shanghai, China). All reagents can be used without further purification.

### 2.2. Preparation and characterization of composite microspheres

#### 2.2.1. Synthesis of GelMA-PP

45 mM imidazole and 16 mM EDC•HCl were dissolved in distilled water and adjusted to pH 6.0 using 1 mol/L HCl. Sodium hexametaphosphate was then added at a final concentration of 3.3 mM. After readjusting the pH to 6.0 using 1 mol/L NaOH, the aqueous mixture was maintained at room temperature for 1.5 h and subsequently purified through ethanol precipitation. The product was lyophilized for 72 h, and imidazole-modified PolyP (PolyP-Im) was obtained as a white powder. Then, 143 mL of GelMA aqueous solution (3.5 mg/mL) was mixed with a 0.1- to 1.0-fold molar excess of PolyP-Im. The solution was reacted at 50 °C for 5 h after adjusting the pH to 8.5 using 1 mol/L NaOH and was subsequently purified through dialysis (MWCO = 6-8kDA) against distilled water at room temperature. The final product, GelMA-PP, was obtained as a white powder through lyophilization for 72 h, and stored at 4 °C.

#### 2.2.2. Preparation of P-GelMA-Ce porous microspheres

According to the literature report [37], injectable porous hydrogel microspheres were prepared by microfluidic technology. In this experiment, P-GelMA porous microspheres were first prepared using this technique. In brief, the aqueous phase (10 wt% GelMA, 2 wt% GelMA-PP, and 0.5 wt% light initiator were uniformly mixed in PBS) and the oil phase (containing 5 wt% Span 80 paraffin oil) were injected into the syringe, and the syringe was connected to a microfluidic device to control the flow rate of the two phases. In this study, the flow rates of the oil phase and the water phase were set to 2000 and 40 μL/min respectively. The obtained monodisperse emulsion drops were crosslinked by UV light in order to obtain microspheres, which were collected in a 250

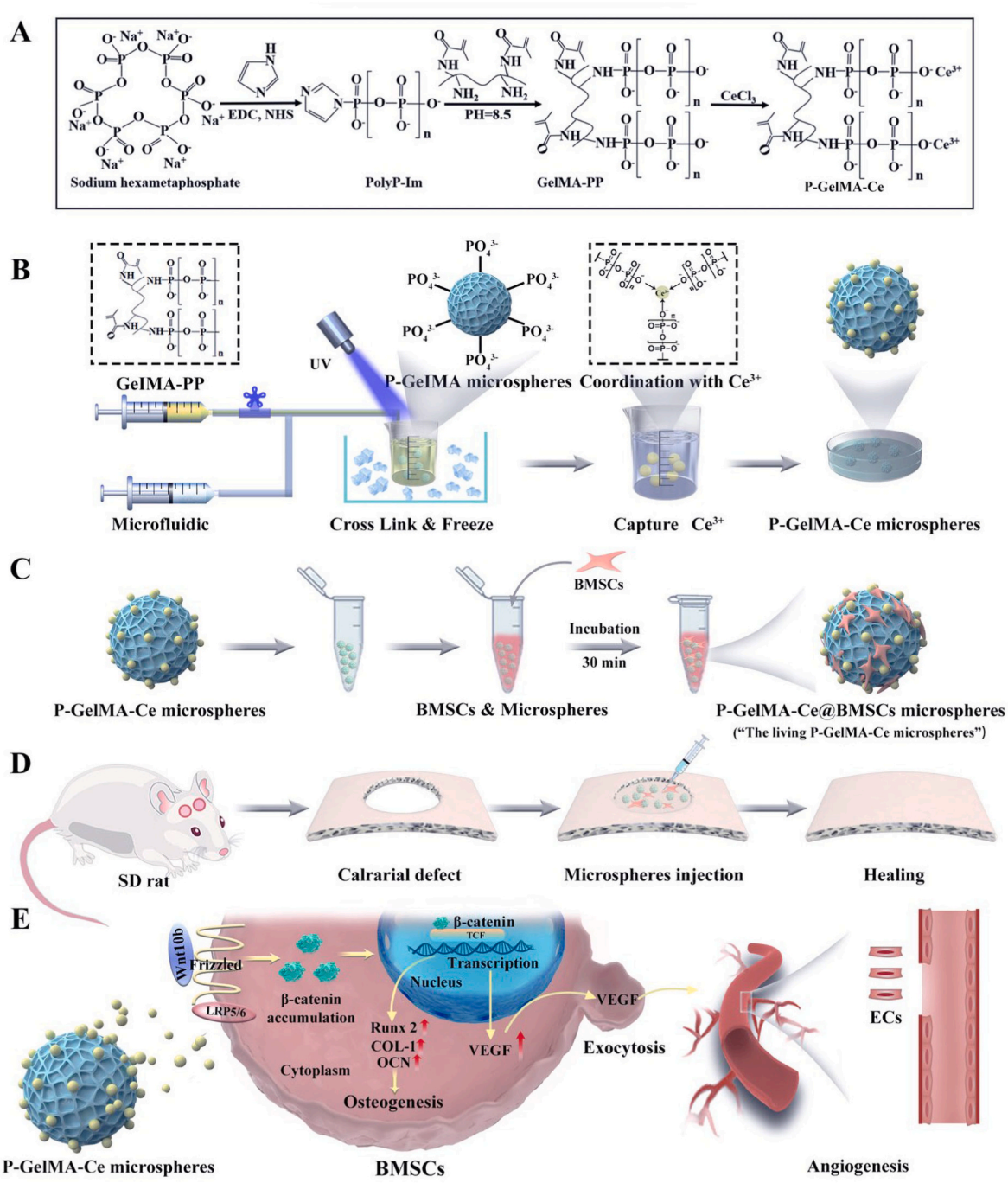


**Scheme 1.** Living and injectable osteoinductive and angioinductive P-GelMA-Ce composite microspheres boost cranial defects repairing of rats. (A) The chemical equation involved in the preparation of P-GelMA-Ce composite microspheres. (B) The fabrication of P-GelMA microspheres using microfluidic technology, and incorporation of $Ce^{3+}$ via the non-covalent coordination chelation to engineer P-GelMA-Ce composite microspheres. (C) The BMSCs-loaded P-GelMA-Ce microspheres, or "the living P-GelMA-Ce microspheres" were further developed through incubation with exogenous BMSCs. (D) In vivo evaluation by injecting composite microspheres into 5 mm rat calvarial defects. (E) Regulation mechanism of osteogenesis and angiogenesis induced by P-GelMA-Ce microspheres.

mL beaker containing an ice water bath at 4 °C and gently stirred overnight. Then the microspheres were washed three times with 75 % alcohol to completely remove the oil phase on the surface, washed three times with $ddH_2O$ and followed by lyophilization and storage. After that, weighing 50 mg of freeze-dried P-GelMA microspheres and 25 mg of anhydrous cerium chloride and placing them in 5 mL of $ddH_2O$ for stirring and mixing for 1 h. Finally, the P-GelMA-Ce porous microspheres were obtained after washing thoroughly with $ddH_2O$, which were freeze-dried and stored for future use.

### 2.2.3. *Evaluation of microspheres degradation rate*

Each group of 10 mg GelMA/P-GelMA/P-GelMA-Ce freeze-dried particles were soaked in 5 mL PBS solution at 37 °C and digested with type II collagenase at a concentration of 0.2 %. Collagenase solution was supplemented every 2 days to maintain enzyme activity. Then, the microspheres were measured the residual weight after lyophilization and dissolved them again in the collagenase solution at different time points (2, 4, 6, 8, 10 weeks). The remaining solid weight was compared with the initial weight. The same method was used to evaluate the degradation of microspheres in pure PBS solution. This experiment was repeated

three times.

#### 2.2.4. Ion release experiment in vitro

According to the literature [38], the release degree of metal ions from hybrid composites in buffer solution was measured by inductively coupled plasma atomic emission spectrometry (ICP-OES/MS, Aglient 7850, USA). Briefly, P-GelMA-Ce microspheres were immersed in 15 mL centrifuge tubes containing 10 mL PBS solution at 0.2 % concentration of type II collagenase, oscillated (100 rpm) at 37 °C and incubated for up to 4 weeks. Fresh collagenase was replenished every 2 days to maintain enzyme activity. At different time points (days 1, 3, 7, 14, 21, and 28), 5 mL of solution was collected from the centrifuge tube and supplemented with the same volume of fresh Tris-HCl buffer. The release of cerium ions from P-GelMA-Ce microspheres in simple PBS solution was measured by the same method.

#### 2.2.5. Characterization of composite microspheres

The physicochemical properties of GelMA, P-GelMA and P-GelMA-Ce composite microspheres were characterized. Phase contrast optical microscope (PCOM, Nikon, Japan) was used to observe the shape and particle size of each group of composite microspheres, and Image J software was used for semi quantitative statistical analysis to draw the particle size distribution map. The surface morphology of the lyophilized composite microspheres was observed using a scanning electron microscope (SEM, sigma 300, Zeiss, Germany) with an accelerating voltage of 5 kV. Before observation, all samples were directly attached to the porous carbon coated copper grid and sputter-coated for 90 s using a gold sputter coater (QUOREM, Q150R Plus, UK). $^{31}$P nuclear magnetic resonance ($^{31}$P NMR; JNM-ECS400 from JEOL, Japan) was used to characterize whether polyphosphate has been grafted onto GelMA microspheres. An energy dispersive spectrometer (EDS, Zeiss, Germany) was used to examine the element distribution within the surface of the composite microspheres. The chemical functional groups of various microspheres were characterized by Fourier transform infrared spectroscopy (FTIR, Thermo Scientific, USA). The spectra were collected in transmission mode in the wavenumber range of 4000 to 500 cm$^{-1}$.

### 2.3. Cell acquisition and culture

In this experiment, all animal experiments strictly comply with the regulations and laws of China and meet the requirements of the ethics committee of Soochow University. Rat bone marrow mesenchymal stem cells (BMSCs) and Human umbilical vein endothelial cells (HUVECs) were used to study the osteogenesis and angiogenesis of Cerium Phosphate GelMA microspheres in vitro, respectively. According to the previously reported method [39], BMSCs were isolated from SD rats (male, 4 weeks, 80–110 g), and only 2–5 passages of cells were used for in vitro cell culture experiments. Briefly, the femurs were first soaked with 10 % penicillin-streptomycin (PS, Gibco, USA) for 5 min, then washed repeatedly with PBS for three times, and then treated with Alpha modified Eagle's medium ( α-MEM, Procell, China) repeatedly rinsed the femoral bone marrow cavity, and then collected the washed contents for centrifugation (1500 rpm, 5 min). The obtained cell pellet was resuspended in a solution containing α- MEM, supplemented with 10 % fetal bovine serum (FBS, Gibco, USA) and 1 % PS, and then cultured in an incubator at 37 °C and 5 % $CO_2$ partial pressure to attach bone marrow mesenchymal stem cells. The attached BMSCs were routinely passaged. After reaching 80 % confluence, they were treated with 0.25 % trypsin- EDTA (Gibco, USA) solution. In addition, HUVECs were obtained from the Shanghai cell bank of the Chinese Academy of Sciences and cultured in Dulbecco's modified Eagle's medium (DMEM, Procell, China) supplemented with 10 % FBS and 1 % PS. All cell processing procedures were performed in a sterile laminar flow hood. The medium was changed every 3 days.

#### 2.3.1. 4Evaluation of cell biocompatibility

Rat bone marrow mesenchymal stem cells were used as experimental materials to study the biocompatibility of composite microspheres. For the live dead staining experiment, BMSCs were co-cultured with lyophilized 4 mg of GelMA/P-GelMA/P-GelMA-Ce composite microspheres at the cell density of $4 \times 10^5$/mL for 30 min, and then transferred to a 20 mm diameter cell culture dish (Nest, 801001, China) for co-culture. The composition of the cell culture medium was 90 % α-MEM, 10 % FBS and 1 % PS. The biocompatibility of the composite microspheres was detected with the Live-Dead Cell Staining Kit (Biovision, USA). The microspheres were co-cultured with BMSCs in a constant temperature incubator (Thermo Scientific, USA) at 37 °C and 5 % $CO_2$ partial pressure for 1, 3, 5 days, and then stained according to the kit instructions. After washing the dye solution with PBS, the microspheres complex was evaluated by a fluorescence inverted microscope (Zeiss, Germany). Cell Counting Kit-8 (CCK-8) methods: CCK-8 Kit (Beyotime, China) was used to evaluate the cytotoxic effect of the material itself on BMSCs. Cells were seeded in 96 well plates at the seeding density of $2 \times 10^4$/mL, and 20 μL of CCK-8 reagent was added to each well at 1, 3, and 5 days for incubating 2 h, then 100 μL culture solution was drawn from each well to a new 96 well plate, and the absorbance was measured at 450 nm with a microplate reader.

### 2.4. Evaluation of in vitro osteogenesis

#### 2.4.1. Alkaline phosphatase staining experiment

Alkaline phosphatase (ALP) staining was used as an early osteogenic marker to determine the osteogenic differentiation of BMSCs in vitro. A density of $5 \times 10^4$/well of BMSCs were seeded on a 24 well plate containing 1 mL α-MEM complete medium and co-cultured with 4 mg of GelMA/P-GelMA/P-GelMA-Ce composite microspheres. Osteogenic inducer (50 μg/mL ascorbic acid, 10 mm β-Sodium glycerophosphate and $10^{-4}$ mm dexamethasone) was added into medium with the cells adherent and grown for 1 day. The medium was changed every 3 days. After 7 days of culture, the cells were washed twice with PBS, fixed with 4 % paraformaldehyde for 30 min, then stained with ALP Staining Kit (C3206, Beyotime, China) for 1 h at room temperature, washed twice with PBS after removing the dye, and finally observed and photographed under the light microscope. Image J software was used to quantitatively analyze the images and calculate the area of ALP positive area.

#### 2.4.2. Alizarin Red S staining experiment

Alizarin Red S (ARS) staining was used as a late osteogenic marker to evaluate the effect of various microspheres on extracellular matrix (ECM) calcium deposition. Cells were seeded and cultured in the same manner as the ALP assay. After 14 days of culture, cells were fixed with 4 % paraformaldehyde solution for 30 min and then washed twice with PBS. Followed by staining with 2 % ARS (C0138, Beyotime, China) for 15min at room temperature. Subsequently, the excess dye was washed away with PBS and the stained samples were photographed under the optimal microscope. Then the culture plate was treated with 10 % cetylpyridinium chloride (Sigma-Aldrich) for 30 min, and the absorbance was measured at 570 nm for quantitative analysis.

### 2.5. Evaluation of in vitro angiogenesis

#### 2.5.1. Tube formation assay

In order to valuing the angiogenesis capacity of HUVECs in vitro, a tube forming assay was conducted. In short, the 96-well plates were first pre-cooled in a −20 °C refrigerator and the Matrigel (Corning, USA) was stored in a 4 °C freezer for later use. The pre-cooled 96-well plates were placed on ice box, then 50 μl Matrigel was added to each hole and no bubbles were confirmed. The matrix glue in the plates was solidified in a cell incubator at 37 °C for 30 min. Then, the supernatant of GelMA, P-GelMA and P-GelMA-Ce microspheres co-cultured with BMSCs for 24 h was mixed with complete DMEM medium at 1:4 ratio, respectively, and

HUVEC cells were co-cultured at a culture density of $1 \times 10^4$/well for 6 h. Pictures were observed and photographed under a light microscope, and three regions were randomly selected to use ImageJ software to calculate the number of luminal nodes and the total length of the lumen.

#### 2.5.2. Scratch assay

The linear wound scratch model was used to assess HUVECs migration. Briefly, HUVECs were inoculated in 12-well plates at a cell density of $5 \times 10^4$/well. After cell attachment, linear scratches were generated by scraping in each well using a p200 pipette tip. The supernatant of each group of microspheres co-cultured with BMSCs for 24 h was mixed with DMEM medium (serum-free) at a ratio of 1:4 to incubate HUVECs for 24 h after being gently washed with PBS, and then the cells migration was visualized using an optical microscope. The scratch area was measured with ImageJ software, and the scratch healing ratio was obtained by the equation:

$$\text{Scratch healing ratio } (\%) = (A_0 - A_1 \ / \ A_0) \times 100\%$$

Where $A_1$ and $A_0$ were the scratch area of 24 h and 0 h, respectively.

#### 2.5.3. Detection of VEGF

The BMSCs were co-cultured with lyophilized 4 mg of GelMA/P-GelMA/P-GelMA-Ce composite microspheres at the cell density of $4 \times 10^5$/mL for 72 h, and then the supernatant was collected. VEGF levels in the supernatant of cell culture medium were detected using a commercial ELISA kit purchased (ML002862, MLBIO, China) according to the instructions.

### 2.6. RT-qPCR

Firstly, BMSCs were co-cultured with composite microspheres of 20 mg each group at the density of $2 \times 10^5$/well in a 6-well plate containing 2 mL α-MEM complete medium. Osteogenic inducer (50 μg/mL ascorbic acid, 10 mm β-Sodium glycerophosphate and $10^{-4}$ mm dexamethasone) was added into medium with the cells adherent and grown for 1 day. The expression of osteogenic related genes such as Collagen I, Runx2, Osterix and OCN were detected by real-time quantitative polymerase chain reaction (RT-qPCR) after 7 days of osteogenic induction. Trizol (Beyotime, China) reagent was added to extract total RNA from cells, and the concentration of purified total RNA was determined using the NanoDrop spectrophotometer (Thermo Fisher Scientific, USA). Subsequently, complementary DNA (cDNA) was reverse transcribed using the Hiscript III RT Supermix reverse transcription kit following the manufacturer's protocol. Next, real-time quantitative polymerase chain reaction was performed using ABI step one plus RT-qPCR system (Applied Biosystems, USA) and SYBR Green RT-PCR Kit (Takara, Japan). Each of the above steps is carried out in strict accordance with the reagent instructions. Primer sequences for each gene are shown in supporting information in Table S1.

### 2.7. Western blotting assay

The cell culture method is consistent with the above RT-qPCR method part. Total protein was extracted with RIPA lysis buffer (Sigma-Aldrich) containing protease inhibitor cocktail in ice-water bath, and the concentration of schizolytic total protein was detected by BCA Protein Kit (Beyotime, China). Protein samples were separated by SDS-PAGE gel electrophoresis after boiling for 5 min (95 °C) and transferred to PVDF membrane. Then, the PVDF membrane was incubated with primary antibodies Collagen I (ab6308, Abcam, UK), Runx2 (ab76956 , Abcam, UK), Osterix (ab209484, Abcam, UK), OCN (ab133612, Abcam, UK) , VEGF (ab52917, Abcam, UK) and Wnt10b (ab70816, Abcam, UK) overnight at 4 °C. All primary antibodies were diluted 1:1000. The membrane was incubated with horseradish peroxidase (HRP) labeled secondary antibody for 1 h at room temperature. The secondary antibody was diluted 1:2000. The free secondary antibody was removed after washing three times with TBST. And then the chemiluminescence system was used for detection and imaging. Finally, Image J software was used to quantify the gray value of the bands.

### 2.8. Immunofluorescence staining analysis

BMSCs were mixed with freeze-dried 4 mg of GelMA/P-GelMA/P-GelMA-Ce composite microspheres at the cell density of $4 \times 10^5$/mL for 30 min, and then transferred to a 20 mm diameter cell culture dish (801001, NEST, China) for co-cultivation. After 7 days of culture osteogenic inducer medium, the cells were fixed with 4 % paraformaldehyde for 30 min at room temperature. After washing twice with PBS, the cells were permeabilized with Triton X-100 (P0096, Beyotime, China) for 15min, and then incubated with immunostaining blocking solution (P0102, Beyotime, China) for 60 min. Next the cells were incubated with antibody collagen I (ab6308, 1:500, Abcam, UK) , VEGF (ab52917, 1:500, Abcam, UK) and Wnt10b (ab70816, 1; 500, Abcam, UK) overnight at 4 °C followed by incubating for 1 h with fluorescent secondary antibody at room temperature in the dark, washed with PBS and stained with DAPI for 5 min. Finally, the cells were imaged under a fluorescence inverted microscope.

### 2.9. In vivo regeneration evaluation

#### 2.9.1. Establishment of rat calvaria defect model

This experimental protocol was approved by the Ethics Committee of Soochow University (SUDA20230221A03). 40 male SD rats (6 week, weight 150–180 g) were randomly divided into 5 groups (GelMA, P-GelMA , P-GelMA-Ce, P-GelMA-Ce@BMSCs and control group) with each group of 8 rats. Rats were injected intraperitoneally with 1 % sodium pentobarbital (0.1mL/100 g), fixed in prone position after complete anesthesia, shaved the area of scalp covering the skull top, and scrubbed with disinfectant (Betadine). Then, the full-thickness incision with a length of about 1.5 cm was made on the scalp to expose the skull, and the full-thickness bilateral bone defect of the sagittal suture with a diameter of 3 mm was established of the sagittal suture by a high-speed skull drill. BMSCs were co-cultured with lyophilized 10 mg of P-GelMA-Ce composite microspheres at the cell density of $1 \times 10^6$/mL for 30 min, and then transferred to a 20 mm diameter cell culture dish (Nest, 801001, China) and co-incubated for 3 days. Finally, each group of lyophilized microspheres (GelMA, P-GelMA, P-GelMA-Ce group) and co-cultured P-GelMA-Ce@BMSCs composite microspheres were dispersed in PBS solution at 10 mg/mL and injected into the skull defect through the 1 mL syringe (20G). Each bone defect area was injected with microspheres of 100 μL. Penicillin was given postoperatively to prevent infection.

#### 2.9.2. Micro-CT analysis

Rats were sacrificed at the 4th and 8th week after microsphere implantation, and rat skulls were fixed in 4 % paraformaldehyde for 24 h. Micro CT (Skyscan1076, Bruker, Belgium) scanning and three-dimensional reconstruction were used. Scanning parameters: voltage 43 kV, current 180 μA, scanning time 450 ms, pixel resolution 12.6 μm. After scanning, the acquired 2D slices were converted into 3D models using SkyScan programs (NRecon, DataViewer, CTAn, and CTvol). A circular region of interest (ROI) with a radius of 2.5 mm was selected at the center of the defect area of each specimen for analysis. The bone tissue volume/total tissue volume (BV/TV), bone mineral density (BMD), trabecular thickness (Tb. Th), and trabecular separation (Tb. Sp) were quantitatively analyzed.

#### 2.9.3. Histological analysis

The rat skull specimens from each group were fixed in 4 % paraformaldehyde for 48 h after Micro-CT scanning, then decalcified with 10 % ethylenediaminetetraacetic acid (EDTA) buffer solution (pH = 7.4)

for 4 weeks. The EDTA solution was changed twice a week. 5 μm thick paraffin slices were prepared after decalcification, gradient alcohol dehydration, paraffin embedding. Samples were then stained with hematoxylin and eosin (H&E) staining, Masson's trichrome staining in order to observe the trabecular morphology of the new bone and the distribution of osteoblasts.

#### 2.9.4. Immunohistochemical staining

The deparaffinized sections were first soaked in 3 % $H_2O_2$ for 30 min, then incubated with 0.25 % trypsin-EDTA (Gibco, USA) in an oven at 37 °C for 1 h, and then blocked with 1 % bovine serum albumin (BSA, Sigma-Aldrich) at room temperature for 30 min. These slices first were incubated with primary antibody Collagen I (ab308455, 1:500, Abcam, UK) and VEGF (ab52917, 1:500, Abcam, UK) overnight at 4 °C, then washed with PBS and incubated with HRP-labeled goat anti-rabbit secondary antibody (A0208, 1:200, Beyotime, China) at room temperature for 1 h, and lastly incubated in DAB solution for coloring. Fluorescence inverted microscope (Zeiss, Germany) was used to image them and observe the expression of osteogenic protein at the tissue level. Finally, the content of type I collagen was measured by Image J software and VEGF expression level was assessed by counting the number of new vessels.

### 2.10. Statistical analysis

All data were collected from at least three samples and expressed as mean ± standard deviation (mean ± SD). One way analysis of variance (ANOVA) and Tukey's post hoc test were used for multiple comparisons, and student's *t*-test was used to compare the mean of two groups. $^{*}P < 0.05$, $^{**}P < 0.01$, and $^{***}P < 0.001$ were considered statistically significant.

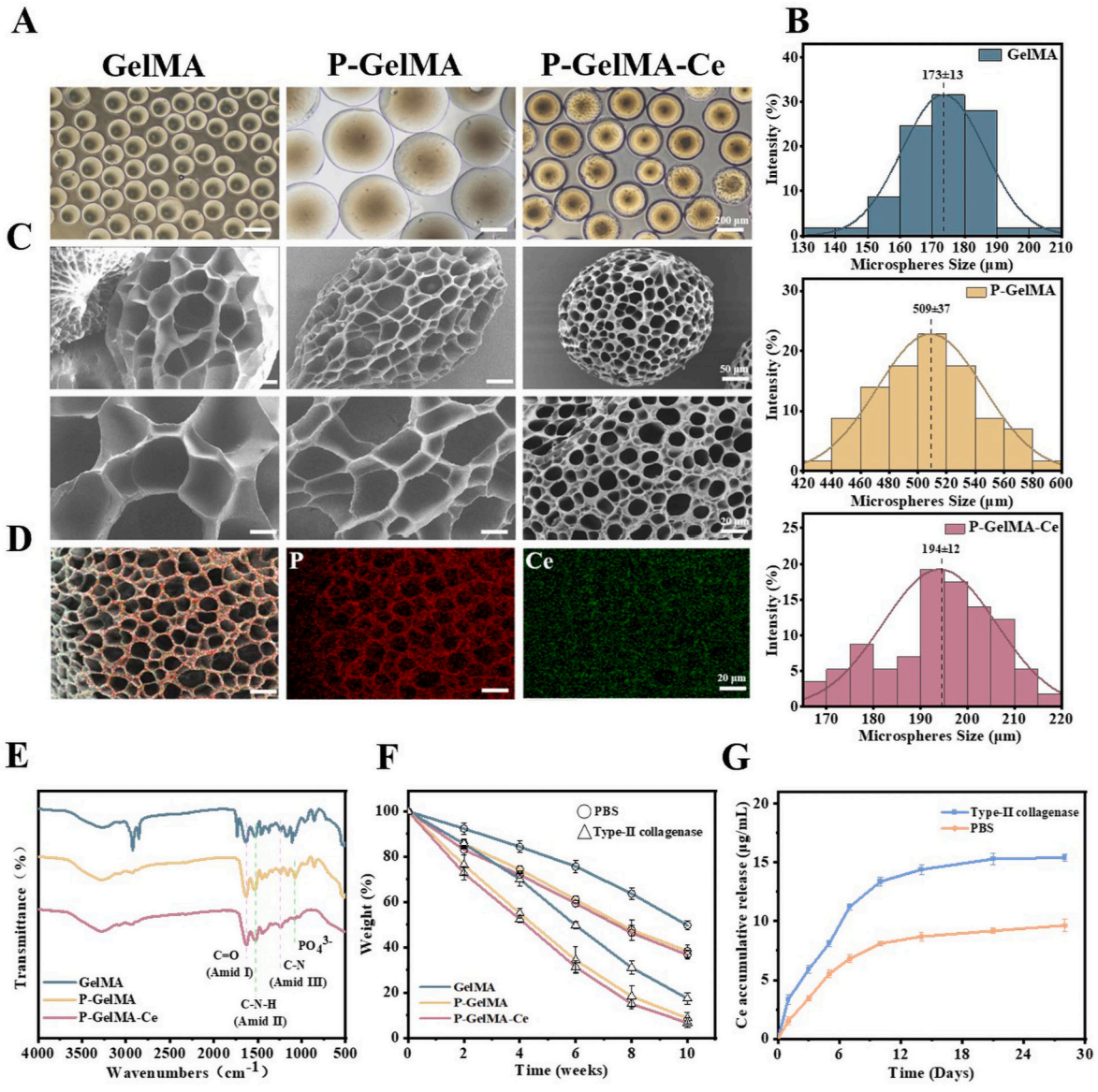


**Fig. 1.** Characteristics of composite microspheres. (A) Microscopic images of GelMA, P-GelMA and P-GelMA-Ce microspheres. (B) Diameter distribution of composite microspheres. (C) Typical scanning electron microscope images of GelMA, P-GelMA, and P-GelMA-Ce microspheres under different magnifications. (D) Uniform distributions of phosphonates and captured $Ce^{3+}$ on P-GelMA-Ce microspheres. (E) FTIR spectra of different microspheres. (F) The degradation curves of different microspheres in different environments over time. (G) In vitro release curves of $Ce^{3+}$ of the P-GelMA-Ce microspheres under different environments.

## 3. Results and discussion

### 3.1. Preparation and characterization of P-GelMA-Ce microspheres

The hierarchical porosity structure and bioactive constituents of artificial biomaterials make an active difference in determining their efficacy in bone defect repair and new bone regeneration [40,41]. The GelMA microspheres possess hierarchical porosity structure that provides favorable microchannels for cellular migration, nutrient transportation, and the development of bone formation [42]. Interestingly, healthy bones naturally contain rare earth elements such as cerium (Ce), lanthanum (La), and ytterbium (Yb), with their accumulation varying with age [43]. Recent research efforts have focused on incorporating bioactive inorganic ions, including cerium ($Ce^{3+}$) and phosphate ($PO_4^{3-}$), into various bone scaffold materials to enhance osteoblast function [44–46]. In our study, highly monodisperse composite hydrogel microspheres (P-GelMA) were prepared using GelMA-PP as the raw material, employing microfluidic technology. The microspheres were created by segmenting the GelMA-PP water phase with an oil phase span of 80, leading to the formation of uniform droplets. Subsequent crosslinking under ultraviolet light and an ice water bath yielded the microspheres. The droplet diameter could be controlled by adjusting the flow ratio of the oil phase ($Q_O$) and water phase ($Q_A$) via the syringe pump [47]. The P-GelMA microspheres were subsequently subjected to cerium ion chelation via noncovalent coordination, resulting in the formation of P-GelMA-Ce hydrogel microspheres. Both GelMA and P-GelMA microspheres, as well as the P-GelMA-Ce composite microspheres, exhibited a spherical shape with high monodispersity when observed under the bright-field microscope. Due to their inherent porous structure, the microspheres exhibited gray coloration with uniform texture and smooth boundaries (Fig. 1A). The average diameters of these microspheres were measured as 173 ± 13 μm, 509 ± 37 μm, and 194 ± 12 μm, respectively (Fig. 1B). The injectability of these particles was enhanced due to their specific particle size, allowing for their administration through the narrow aperture of a medical syringe. This characteristic enables the facilitation of less invasive therapeutic interventions. The dramatic increase in particle size observed in the P-GelMA microspheres could be attributed to the enhanced hydrophilicity resulting from incorporating polyphosphate. Scanning electron microscopy (SEM) examination revealed that the surface and interior of each group of lyophilized hydrogel microspheres featured the regular porous structure, connecting the interior and exterior spaces. This porous architecture is advantageous for nutrient and oxygen transport (Fig. 1C). In addition, the presence of porous structure in microsphere scaffolds enhances the surface area available for cell adhesion and loading capacity, in contrast to microsphere scaffolds lacking porosity. The significance of the microspheres' porosity should be acknowledged as it plays a pivotal role in determining the quantity of loading units [48]. The presence of porous structure resulted in an increased surface area, which in turn facilitated cell adherence and improved loading capacity as compared to microsphere scaffolds lacking porosity. The pore size of P-GelMA-Ce microspheres was relatively small compared to the other two groups, attributable to cerium ion modification. Additionally, the $^{31}P$ NMR spectrum confirmed the presence of polyphosphate in the absorption peak of P-GelMA microspheres at 7.6 ppm (Fig. S1A), while energy dispersive spectroscopy (EDS) elemental analysis demonstrated even distribution of P and Ce elements on the surface of P-GelMA-Ce microspheres (Fig. 1D). Chemical bond analysis via Fourier transform infrared spectroscopy (FTIR) further supported the successful grafting of polyphosphate onto GelMA microspheres, and the results were shown in Fig. 1E. All microspheres had a characteristic amide I peak (1633 $cm^{-1}$), amide II peak (1532 $cm^{-1}$) and amide III peak (1241 $cm^{-1}$). Compared with GelMA microspheres, the P-GelMA and P-GelMA-Ce composite microspheres showed a characteristic peak of $PO_4^{3-}$ at 1078 $cm^{-1}$. Consequently, this research offers multifaceted confirmation that polyphosphate was effectively integrated into GelMA microspheres, facilitating the successful capture of $Ce^{3+}$.

Proper degradation of porous hydrogel microspheres is imperative to facilitate cell migration and infiltration. GelMA, P-GelMA, and P-GelMA-Ce microspheres were each subjected to degradation experiments in PBS solutions, both with and without the presence of 0.2 % type II collagenase. As illustrated in Fig. 1F, the degradation of P-GelMA-Ce occurred gradually and steadily in the collagenase environment, with degradation rates of 35 ± 2 % and 72 ± 3 % observed at the 4th and 8th weeks, respectively. The inherent hydrophilicity of GelMA prior to modification was limited, resulting in a slow degradation rate. Following polyphosphoric acid grafting, the degradation rate increased, likely attributed to the cleavage of amide bonds and an elevation in hydrophilicity. Despite this accelerated degradation, it remained a controlled and balanced process. Excessive degradation can result in enlarged mesh sizes, diminishing the deposition of the extracellular matrix (ECM), which is detrimental to cell proliferation and ECM formation [49]. In comparison to the PBS environment, the degradation rate of microspheres in each group was notably enhanced under collagenase conditions, with approximately a 30 % increase observed at the 10th week (Fig. S1B). Degradation in the presence of collagenase better simulates the in vivo degradation process of microspheres. To investigate the in vitro release of cerium ions from P-GelMA-Ce composite microspheres after immersion in Tris-HCl buffer solution, inductively coupled plasma atomic emission spectrometry (ICP-OES/MS) was employed (Fig. 1G). The release of cerium ions from P-GelMA-Ce microspheres exhibited a responsive pattern to collagenase. Over the initial 10 days, the concentration of cerium ions displayed a prominent increase. Subsequently, the release curve reached a plateau, and the release of cerium ions gradually decreased, stabilizing at the 21st day. The release concentration of cerium ions increased from 3.3 ± 0.4 μg/mL on the 1st day to 15.4 ± 0.3 μg/mL on the 28th day. Notably, collagenase facilitated the release of cerium ions from microspheres compared to the PBS environment (Fig. S1C). Without grafting polyphosphate , the release of cerium ions from freeze-dried GelMA hydrogel microspheres mixed with anhydrous cerium chloride (5 mg/mL) for 1 h showed a sudden release process, and reached the plateau stage on the fifth day. However, the cumulative release of cerium ions ( 15.6 ± 0.45 μg/mL ) from GelMA hydrogel microspheres was similar to P-GelMA-Ce microspheres (Fig. S1D).

The current research about *the Ce-containing biomaterials* mainly focuses on the excellent properties of $CeO_2$ concerning their enzyme-like activities, such as wound healing, cancer therapies, bone regeneration, neurological diseases, and treatment of other oxidative stress-related diseases. However, the biotoxicity of $CeO_2$ is the determining factor to influences its applications in living organisms. As a non-degradable nanomaterial, the in vivo metabolic pathway of $CeO_2$ deserves to be discussed further. For example, nanoparticles of 30 nm and below are metabolized by the kidneys, those with sizes of 30–500 nm may be metabolized by the liver and spleen. It is still unknown whether the long-term accumulation of $CeO_2$ in each organ during the above metabolism process will lead to organ pathology [50]. Therapeutic inorganic ions provide a potential solution in this work. For example, cerium ions have specific functions in the body, such as osteogenesis, antibacterial activity, angiogenesis, immune regulation, and potential cancer treatment effects. Consequently, the use of metal ion-loaded biomaterials as potent carriers for controlled release of specific therapeutic ions represents a highly promising strategy in the field of bone tissue engineering.

### 3.2. Biocompatibility evaluation of composite microspheres

To assess the biocompatibility of the modified microspheres, live/dead staining, and Cell Counting Kit-8 (CCK8) detection experiments were conducted on the cell-microsphere complexes. The analysis of live/dead staining findings collected on the 1st, 3rd, and 5th days revealed that the population of bone marrow mesenchymal stem cells (BMSCs) in all experimental groups exhibited an increase in density as the duration

of culture prolonged. Furthermore, the vast majority of cells in each group maintained their viability, while a minority of cells were observed to be non-viable (Fig. 2A and B). Furthermore, CCK8 analysis revealed that the microspheres did not exert any adverse effects on BMSCs' proliferation at any of the time points (Fig. 2C). Collectively, these findings indicated that the composite microspheres utilized in this work exhibited excellent biocompatibility with BMSCs, creating a nontoxic and advantageous microenvironment for cell adhesion.

### 3.3. Evaluation of the in vitro osteogenic effects by P-GelMA-Ce microspheres

In the realm of bone tissue engineering, the development of multifunctional three-dimensional scaffolds incorporating cerium as an additive has garnered significant research attention. Guo's research group, for instance, reported the creation of $CeO_2$ nanoparticles-modified bioglass (Ce-BG) microspheres incorporated into chitosan, resulting in $CeO_2$-doped hollow mesoporous BG scaffolds. The presence of $CeO_2$ in these scaffolds provides active sites that enable the proliferation and osteogenic differentiation of human bone marrow mesenchymal stem cells (hBMSCs). Additionally, the hierarchical porosity structure of these scaffolds proves to be favorable to the development and migration of hBMSCs. In addition, the treatment with scaffolds containing $CeO_2$ led to an increase in the expression of osteocalcin (OCN) and type I collagen (COL-1), both on the protein and the gene levels [51]. In our experiment, P-GelMA-Ce microspheres demonstrated a similar osteogenic effect. To elucidate the osteogenic impact of P-GelMA-Ce microspheres within an in vitro direct culture system, BMSCs were subjected to osteogenic differentiation medium. The initiation of osteogenic differentiation at an early stage results in the upregulation of alkaline phosphatase (ALP) expression, which may be observed by employing ALP staining techniques. In the context of bone regeneration, the scaffold's ability to induce biomineralization serves as a pivotal indicator of its osteogenic potential, with Alizarin Red S (ARS) staining used to evaluate the degree of mineralization. ALP staining images (day 7) revealed that the bright blue area in the P-GelMA-Ce group was notably more pronounced compared to the GelMA group, followed by the P-GelMA group. Quantitative analysis of ALP staining further confirmed the remarkably enhanced osteogenic differentiation ability of the P-GelMA-Ce group (Fig. 3A and B). Results from ARS staining (day 14) and subsequent quantitative analysis demonstrated a memorably increase in calcium mineral deposition within the P-GelMA-Ce group, significantly enhancing the osteogenic competence of BMSCs (Fig. 3C and D). Immunofluorescence staining was employed to assess the expression of the osteogenic protein collagen I after 7 days of osteogenic induction. The provided image in Fig. 3E clearly highlighted the differences in fluorescence intensity. Among BMSCs cultured on P-GelMA-Ce microspheres, Collagen I expression was the most pronounced, followed by the P-GelMA group. Semi-quantitative analysis of these fluorescent signals manifested a substantial upregulation of osteogenic protein Collagen I in the P-GelMA-Ce group compared to the GelMA group (Fig. 3F).

In order to provide a more comprehensive understanding of the influence of P-GelMA-Ce microspheres on the expression of osteogenic genes in BMSCs, a range of key osteogenic genes and proteins, namely collagen I (COL1A1), runt-related transcription factor 2 (Runx2), Osterix, and osteonectin (OCN), were evaluated using quantitative real-time polymerase chain reaction (qRT-PCR) and Western blot analysis. The qRT-PCR and Western blot analyses consistently demonstrated statistically significant upregulation of osteogenesis-related genes and proteins in the P-GelMA-Ce group relative to the other experimental groups following a 7-day culture period (Fig. 4A–C). It is important to emphasize that materials that have undergone phosphorylation have features that facilitate their targeting of bone tissue. These materials are

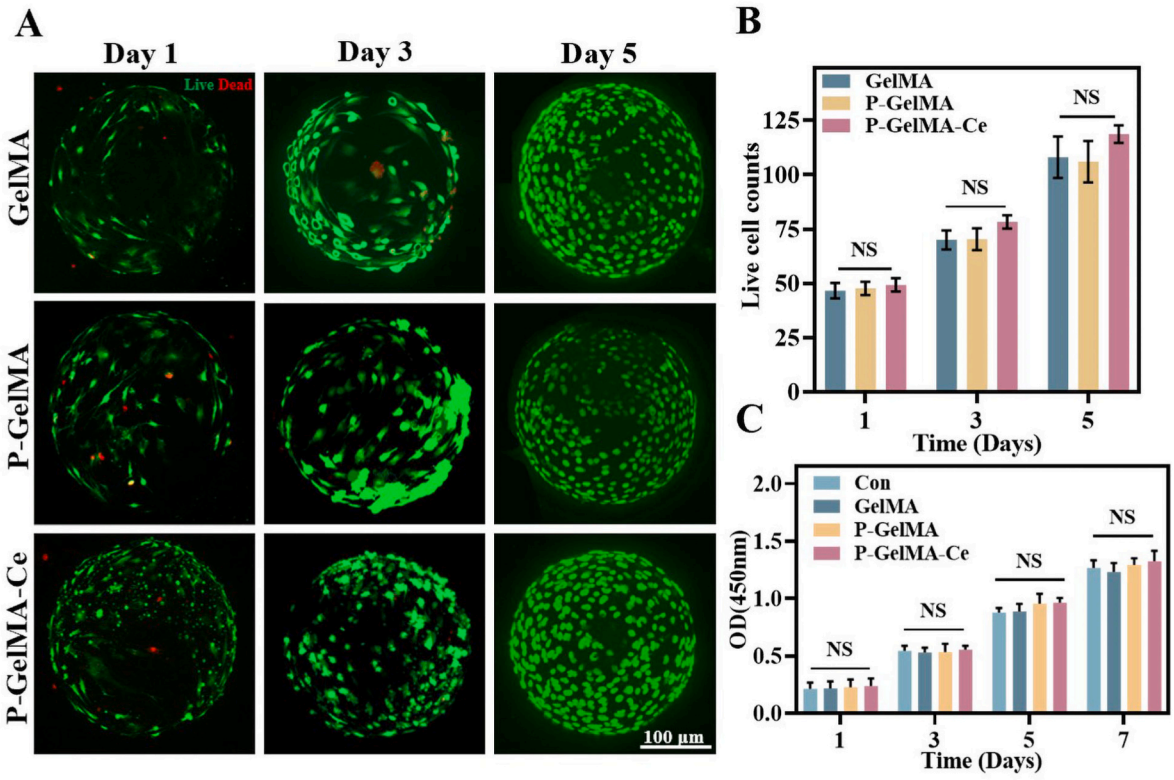


**Fig. 2.** Biocompatibility of composite microspheres. (A) BMSCs were cocultured with composite microspheres for 1, 3, and 5 days and analyzed by live/dead staining. Live cells were green, and dead cells were red. (B) Statistics of the live cell counts of the BMSCs. (C) CCK-8 detected the toxicity of these composite microspheres. (NS, no significant difference; *, $P < 0.05$). (For interpretation of the references to color in this figure legend, the reader is referred to the Web version of this article.)

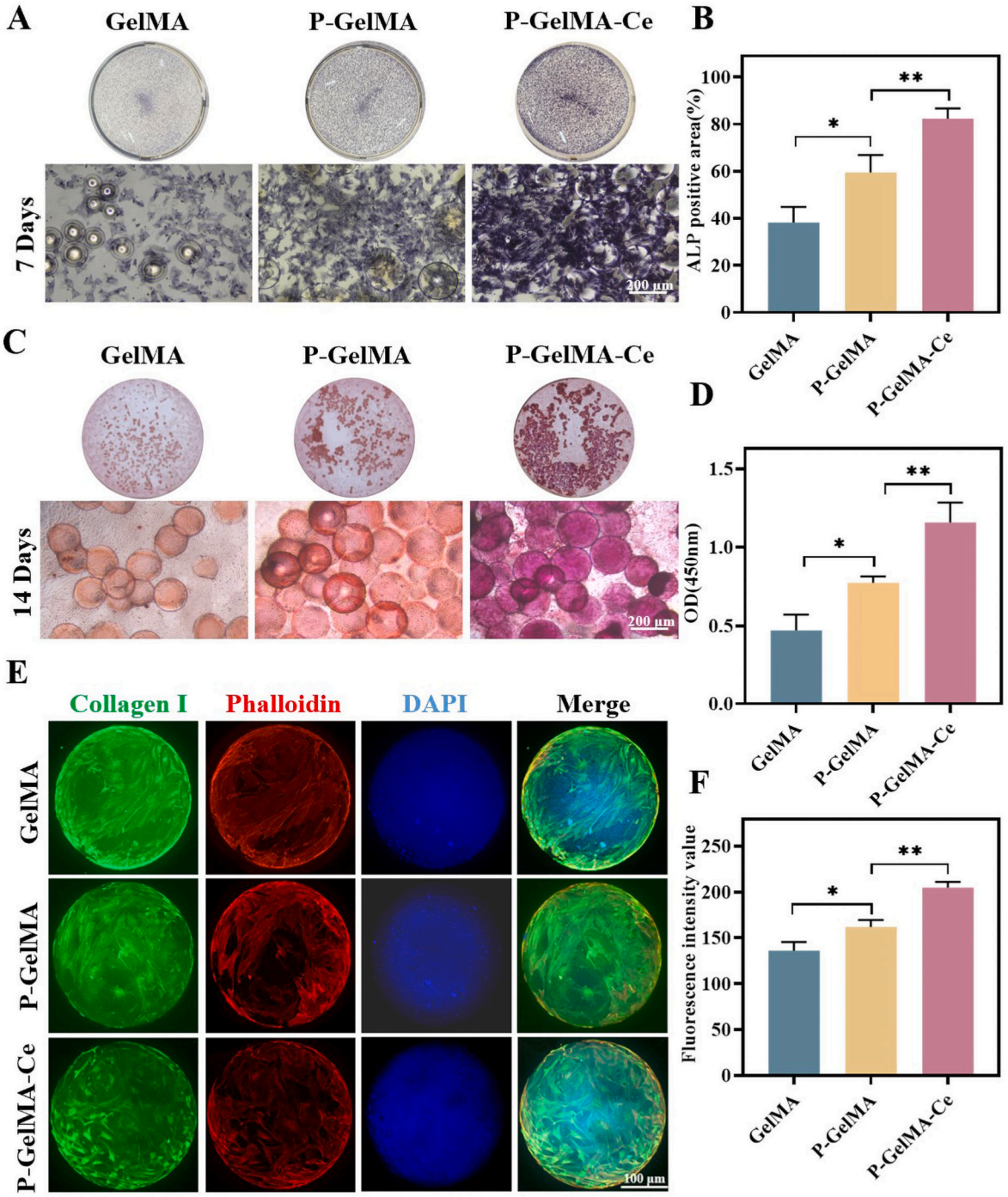


**Fig. 3.** Biomineralization study and osteogenic differentiation of BMSCs cultured on composite microspheres. (A, C) Optical microscopy images showing ALP staining (A) and Alizarin red staining (C) of BMSCs cultured in the presence of different microspheres for 7 days and 14 days in the osteoinductive medium. (B, D) Quantitative analysis of ALP staining and Alizarin Red S staining in different groups. (E) Immunofluorescence staining of Collagen I on different microspheres. (F) Quantitative analysis of osteogenic protein expression using fluorescence density value. (*, $P < 0.05$; **, $P < 0.01$). (For interpretation of the references to color in this figure legend, the reader is referred to the Web version of this article.)

able to attach to hydroxyapatite crystals present in bone, thereby creating active sites that promote the process of bone mineralization [52]. In our study, GelMA-PP served not only as a cerium ion capturer but also exhibited bone-targeting and bone-promoting effects. This phenomenon presents a plausible explanation for the P-GelMA group's capacity to promote osteogenesis to a certain extent.

### *3.4. Evaluation of the in vitro angiogenesis effects by P-GelMA-Ce microspheres*

The provision of sufficient blood supply is of utmost importance in the process of bone regeneration, as it accelerates the delivery of essential nutrients, growth factors, and oxygen required for tissue repair [53,54]. Metal ions, such as zinc, copper, magnesium, and cerium, as well as bioactive compounds like vascular endothelial growth factor (VEGF) and platelet-derived growth factor-BB (PDGF-BB), has the

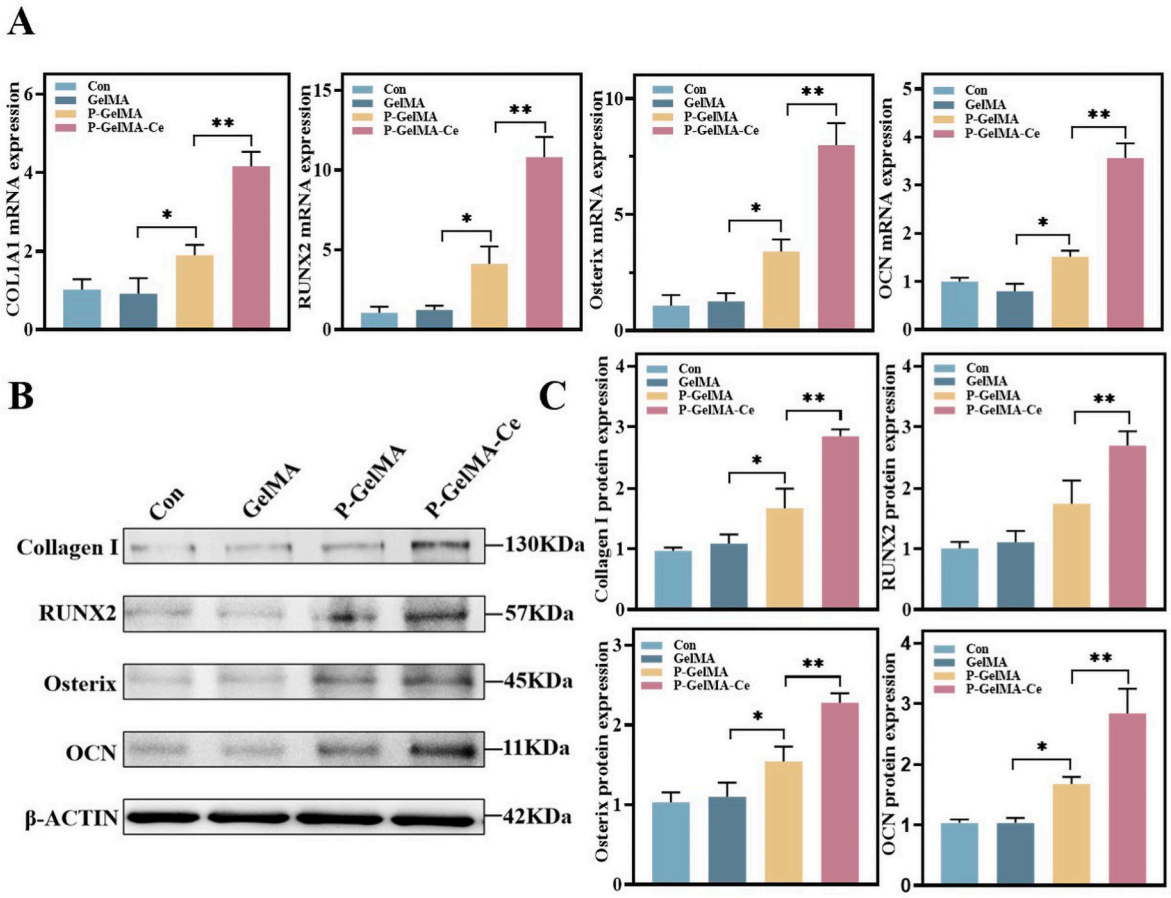


**Fig. 4.** Effect of composite microspheres on the expression of osteogenic genes in BMSCs. (A) Expression analysis of osteogenesis-related genes (COL1A1, RUNX2, Osterix, and OCN). (B, C) Western blot exploring the protein (Collagen I, RUNX2, Osterix, and OCN) expression and performing quantitative analysis. (*, $P < 0.05$; **, $P < 0.01$).

ability to induce the proliferation, migration, and angiogenesis of epidermal and endothelial cells [55–57]. VEGF can induce endothelial progenitor cells (EPCs) to differentiate into mature endothelial cells (ECs) and self-form new blood vessels in the absence of existing vascular support [58]. In the process of vasculogenesis, VEGF is indispensable for the recruitment, maintenance, proliferation, migration and differentiation of endothelial cells. Additionally, bone marrow mesenchymal stem cells release VEGF, facilitating the proliferation and migration of EPCs and ECs through paracrine signaling [59]. Dong et al. reported that cerium nanoparticles promoted the secretion of PDGF-BB and VEGF by BMSCs, subsequently inducing angiogenesis of EPCs, demonstrating the paracrine effect [60]. To directly assess the angiogenic capacity of P-GelMA-Ce microspheres, tube formation experiments were conducted using human umbilical vein endothelial cells (HUVECs). Following a 6-h incubation period, a noteworthy augmentation in the production of endothelial tubes was detected in the P-GelMA-Ce group in comparison to the Control, GelMA, and P-GelMA groups, as depicted in Fig. 5A. The results of quantitative analysis indicated that the P-GelMA-Ce group exhibited a significantly higher number of connections and overall tube length compared to the other groups (Fig. 5B and C). These results demonstrated that the cerium ions released by the composite microspheres possess angiogenic activity. The migratory capacity of HUVECs was evaluated through scratch assays (Fig. 5D and E). After 24 h of incubation, both qualitative and quantitative assessments showed that the remaining scratch area in the P-GelMA-Ce group was significantly smaller than in the other groups, with a scratch area healing rate of approximately 71 %, indicating that cerium ions markedly induced HUVECs' migration. Immunofluorescence staining for VEGF and subsequent quantitative analysis further confirmed that the fluorescence intensity in the P-GelMA-Ce group was substantially stronger than that in the GelMA and P-GelMA groups (Fig. 5F and G). The concentration of supernate VEGF in the microspheres&BMSCs co-culture system was detected by enzyme-linked immunosorbent assay (ELISA). The concentration of VEGF in P-GelMA-Ce group (37.35 pg/mL) was significantly higher than that of the other two groups (Fig. S2A), indicating that $Ce^{3+}$ promoted the secretion of VEGF by BMSCs. Moreover, the expression of the angiogenesis-related protein VEGF was assessed to evaluate the regulatory effect of P-GelMA-Ce microspheres on angiogenesis at the gene level. As Fig. 5H and Fig. S2B depicted, VEGF expression was observably upregulated in the P-GelMA-Ce group. These results demonstrated that P-GelMA-Ce microspheres can enhance the secretion of VEGF by BMSCs, thereby inducing angiogenesis to promote bone regeneration.

### 3.5. *Potential mechanism for promoting bone regeneration by P-GelMA-Ce microspheres*

The study conducted by Luo et al. shed light on CeONPs enhancing the translocation of β-catenin into the nucleus and activating the canonical Wnt pathway. This activation was achieved by the upregulation of B/SIMPLET, a member of the sequence similarity 53 protein family [61]. This discovery is consistent with our findings, as it is widely recognized that the Wnt/β-catenin signaling pathway plays a crucial role in regulating the process of osteogenic differentiation and bone production. The activation of the Wnt signaling pathway facilitates the upregulation of osteoblast-associated genes, including as OCN, ALP, and

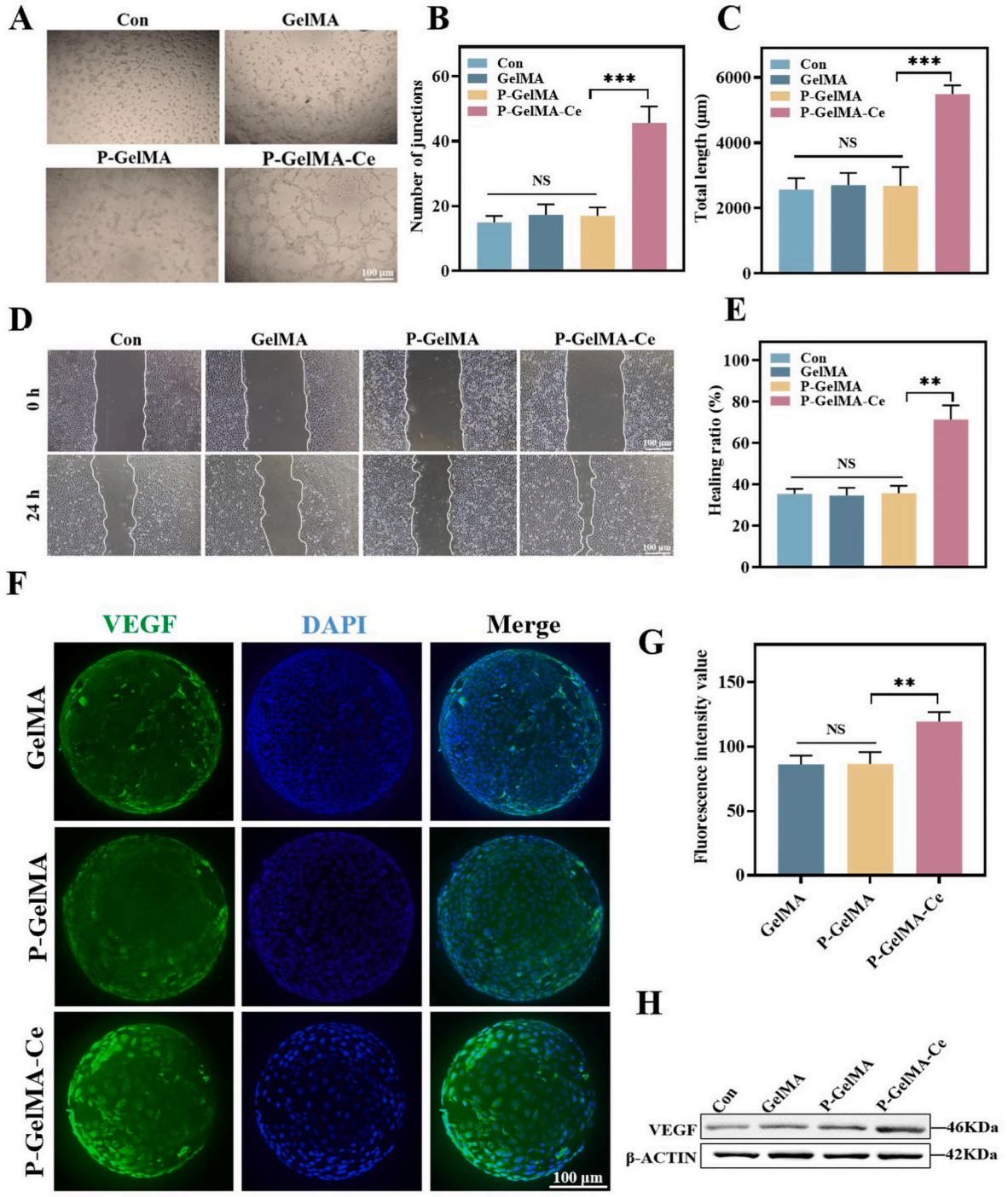


**Fig. 5.** Angiogenesis properties of different microspheres in vitro. (A) Representative microscopy images of the tube formation in the Con, GelMA, P-GelMA, and P-GelMA-Ce groups. The quantitative analysis of (B) number of nodes and (C) tube length of HUVECs in these different groups. (D) Representative microscopic images and (E) quantified analysis for the migrated HUVECs in the Con, GelMA, P-GelMA, and P-GelMA-Ce groups incorporated in the scratch wound healing assay. (E) Immunofluorescence staining of VEGF on different microspheres. (F) Quantitative analysis of angiogenesis protein expression using fluorescence density value. (G) Western blot exploring the protein VEGF expression. (NS, no significant difference; **, $P < 0.01$; ***, $P < 0.001$).

COL-1 [62]. Moreover, the Wnt/β-Catenin signaling pathway serves a vital function in determining the vascular destiny of mesenchymal cells [63]. Prior research has demonstrated that the Wnt/β-Catenin signaling pathway is of pivotal importance in the processes of angiogenesis and differentiation in the context of development [64]. Based on our results, P-GelMA-Ce microspheres stimulated the secretion of VEGF from bone marrow mesenchymal stem cells (BMSCs), which, in turn, may positively influence the vasculogenesis of endothelial progenitor cells. Hence, it was hypothesized that the incorporation of cerium ions into P-GelMA-Ce microspheres might potentially induce the activation of the Wnt/β-catenin signaling pathway, hence accelerating the process of bone regeneration. The protein expression levels of crucial components within the Wnt signaling pathway were evaluated using the Western blotting technique, as depicted in Fig. 6A and B. The levels of Wnt10b expression in BMSCs that were co-cultured with P-GelMA-Ce microspheres exhibited a notable and statistically significant rise. However,

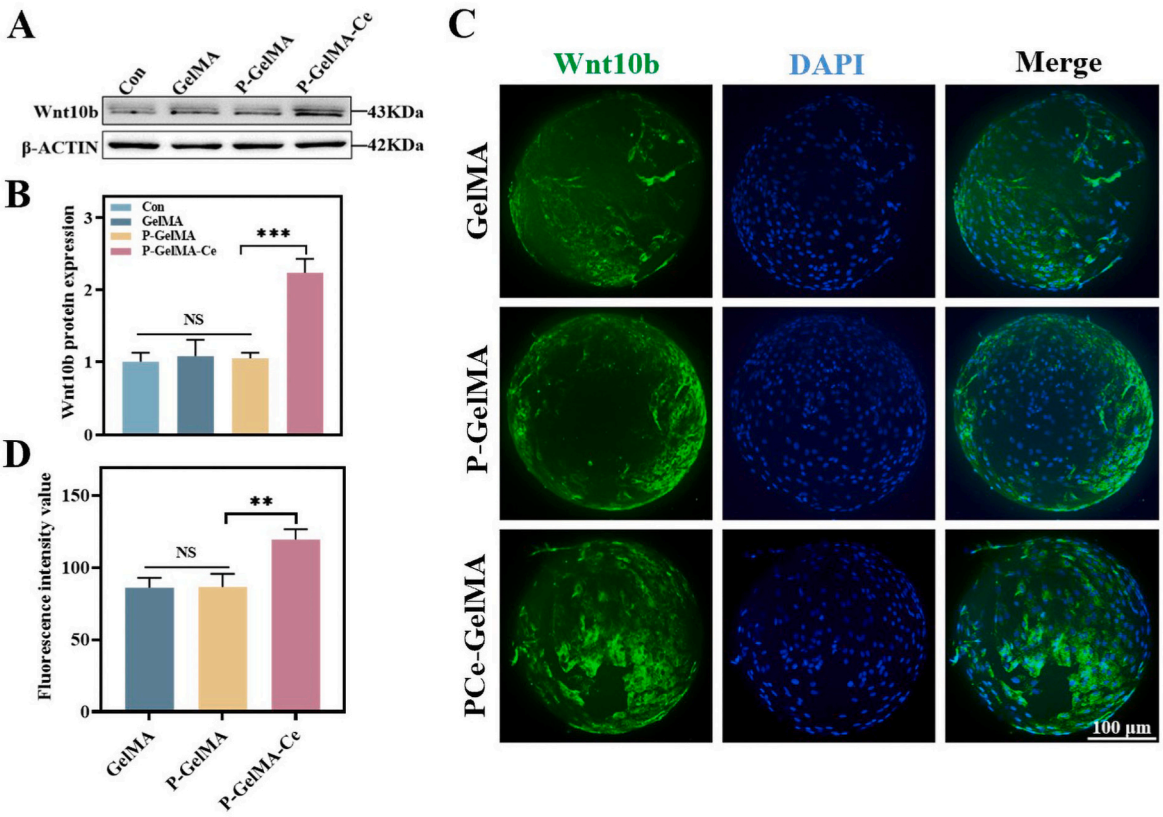


**Fig. 6.** P-GelMA-Ce microspheres promote the calvarial regeneration mechanism. (A, B) Western blot exploring the protein Wnt10b expression and performing quantitative analysis. (C) Immunofluorescence staining of Wnt10b on different microspheres. (D) Quantitative analysis of protein Wnt10b expression using fluorescence density value. (NS, no significant difference; **, $P < 0.01$; ***, $P < 0.001$).

no significant difference in Wnt10b expression was seen in the remaining groups. Immunofluorescence staining images and quantitative analysis further confirmed that the P-GelMA-Ce group could dramatically upregulate the secretion of Wnt10b by BMSCs (Fig. 6C and D). The initiation of the classical Wnt signaling pathway involves the interaction between Frizzled-type transmembrane receptors, low-density lipoprotein receptor-related protein 5 (LRP5) and/or LRP6, and secreted WNTs. This interaction results in the accumulation of β-catenin protein within the cytoplasm, followed by its translocation to the nucleus [65]. In this study, activation of the Wnt/β-catenin pathway promoted the expression of downstream osteogenic genes COL-1, Runx 2 and OCN, as well as stimulated the secretion of VEGF by BMSCs, regulating osteogenic differentiation and angiogenesis to achieve bone regeneration (Scheme 1E).

### 3.6. *P-GelMA-Ce@BMSCs microspheres induces in vivo osteogenic regeneration in calvarial defects*

Animal experiments involving appropriate defect modeling represent a potent method for assessing the potential of scaffolds to induce in situ bone regeneration. In order to assess the efficacy of these composite hydrogel microspheres in promoting bone regeneration, critical-sized calvarial bone lesions were surgically induced in Sprague-Dawley rats (Fig. 7A). As depicted in Fig. 7B–a full-thickness defect with a 3 mm diameter was drilled on each side of the sagittal suture of the rat skull, and GelMA microspheres, P-GelMA microspheres, P-GelMA-Ce microspheres, and P-GelMA-Ce@BMSCs microspheres were injected into the defects. The red arrow indicates an overview of the injected microspheres. The control group did not receive any material injection. The collection of skulls occurred at two specific time points, namely the fourth and eighth weeks following the surgical procedure. To evaluate the process of new bone tissue formation, the utilization of Micro-CT scanning was employed. Transverse images and 3D reconstruction results displayed significant distinctions between the groups. Following a duration of four weeks, a discernible augmentation in newly formed bone tissue was noticed inside the experimental group treated with P-GelMA-Ce@BMSCs. Minimal new bone growth was observed only around the periphery of the lesion site in both the control and GelMA groups. In the P-GelMA and P-GelMA-Ce groups, the bone defects exhibited partial healing with limited new bone formation, and bone mass was relatively low. By the 8th week, the degree of bone repair in each group had improved compared to the 4th week. However, bone repair in the control and GelMA groups remained suboptimal, indicating limited self-repair capabilities for critical-sized bone defects. Although a significant area of new bone filled in the P-GelMA group and P-GelMA-Ce group, substantial gaps still existed. The P-GelMA-Ce@BMSCs group achieved nearly complete repair and demonstrated an ideal bone healing effect (Fig. 7C). The results of the quantitative analysis demonstrated that the groups injected with P-GelMA-Ce@BMSCs microspheres and P-GelMA-Ce microspheres exhibited significantly higher values for bone tissue volume/total tissue volume (BV/TV), bone mineral density (BMD), and trabecular thickness (Tb.Th) compared to the other three groups, at both the 4-week and 8-week time points. Additionally, the trabecular bone spacing (Tb.Sp) in these two groups was significantly lower than that observed in the other three groups. It is worth noting that, compared to the P-GelMA-Ce group, the P-GelMA-Ce@BMSCs group exhibited a 25 % increase in BV/TV, a 29 % increase in BMD, a 16 % increase in Tb.Th, and a 25 % decrease in Tb.Sp at 4 weeks. At 8 weeks, BV/TV, BMD, and Tb.Th increased by 40 %, 45 %, and 17 %, respectively, while Tb.Sp decreased by 20 % (Fig. 7D and E). This is attributed to the fact that P-GelMA-Ce@BMSCs microspheres not only promote the adhesion and proliferation of endogenous BMSCs but also

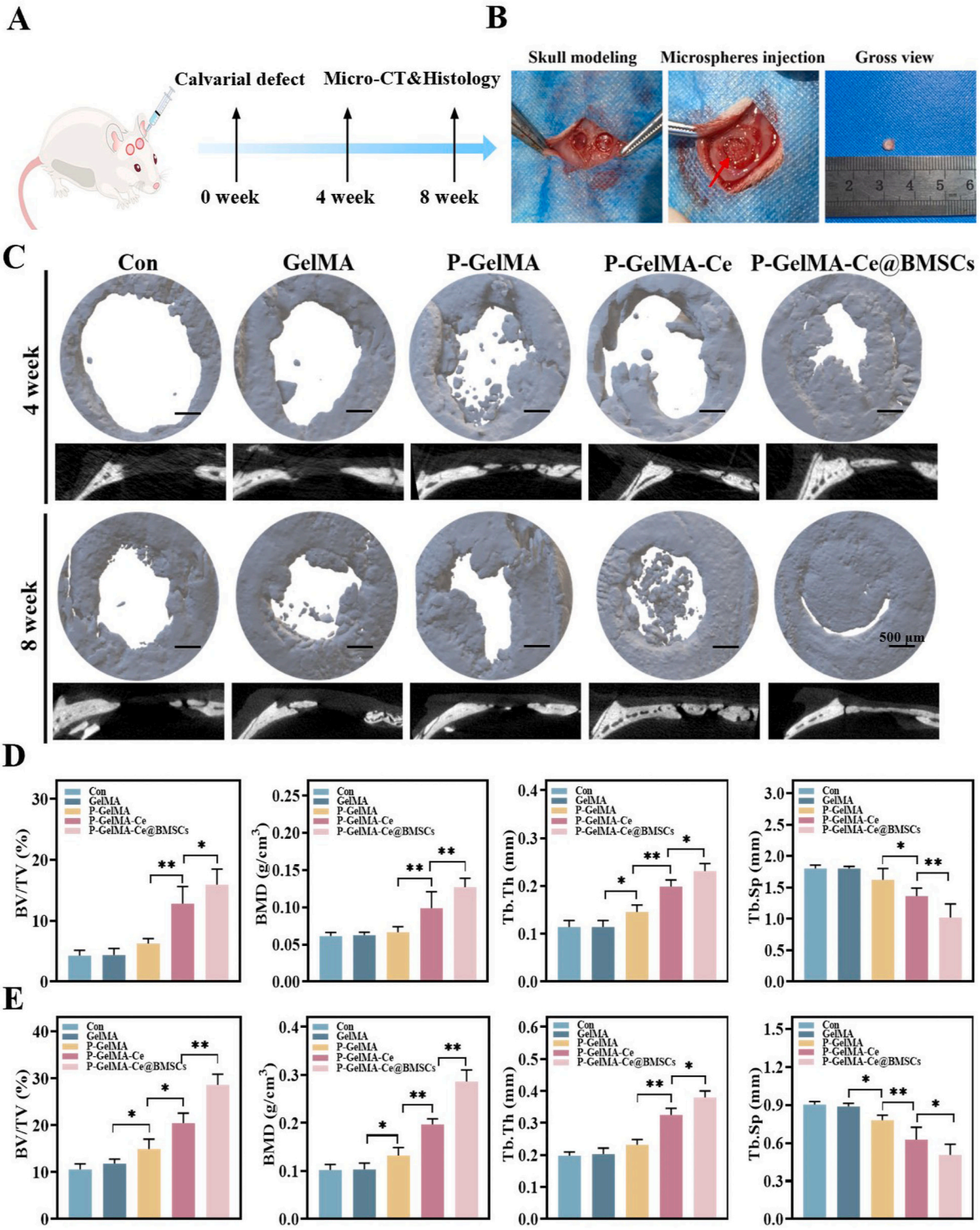


**Fig. 7.** Bone regeneration in the critical-size cranial bone defect of a rat model. (A) Schematic illustration showing the establishment of skull defect model in SD rats. (B) Snapshots of the surgical procedure. (C) Mineralization in the cranial defect area was evaluated using microcomputed tomography (micro-CT) at 4 and 8 weeks. (D, E) Quantitative analysis of the BV/TV, BMD, Tb.Th, and Tb.Sp in different treatment groups of the regenerated bone 4 and 8 weeks after injection. (*, $P < 0.05$; **, $P < 0.01$).

load exogenous BMSCs to enhance cell-ECM and cell-cell interactions, bolster paracrine effects, and thereby further stimulate bone regeneration and repair.

In line with the outcomes of Micro-CT reconstruction and quantitative analysis, histological staining further substantiated the bone regeneration-promoting capabilities of P-GelMA-Ce@BMSCs composite microspheres. HE and Masson staining were conducted at 4 and 8 weeks. HE staining assessed the morphology and tissue margin of the skull defect. No signs of inflammation or osteonecrosis were detected in any of the groups. At the 4th week, early bone regeneration was observable in the control and GelMA groups, accompanied by some loose fibrous tissue at the defect margin. The P-GelMA group exhibited an increase in fibrous tissue and osteoblast aggregation. Notably, new bone formation and increased trabecular thickness were evident in the P-GelMA-Ce and

P-GelMA-Ce@BMSCs groups. The P-GelMA-Ce@BMSCs group additionally displayed signs of neovascularization. By the 8th week, a significant number of osteoblasts were visible in the blank control and GelMA groups, and new bone had started to form at the defect edge. In the P-GelMA group, the fibrous tissue had been replaced by sporadic bone trabeculae. In contrast, the P-GelMA-Ce group exhibited continuous new and mature bone development. Abundant new vessels surrounded the mature bones in the P-GelMA-Ce@BMSCs group (Fig. 8A). Masson staining depicted collagen synthesis and ossification with blue and red colors. At the 4th week, only sparse blue collagen fibers were apparent in the control and GelMA groups. A substantial amount of deeply stained collagen was observed in the bone matrix of the P-GelMA group. Red weaving indicated new bone formation in the P-GelMA-Ce group. The P-GelMA-Ce@BMSCs group exhibited continuous red woven bone, accompanied by an abundance of deeply stained collagen. By the 8th week, the number of collagen fibers had increased in both the control and GelMA groups. In the P-GelMA group, numerous deep-dyed collagen fibers showed sparse braiding. In the P-GelMA-Ce group, newly formed bone had significantly increased and assumed a continuous, dense appearance. The P-GelMA-Ce@BMSCs group displayed mature calcified lamellar bone and neovascularization (Fig. 8B).

Furthermore, histological analysis included collagen I and VEGF immunohistochemical staining. Immunohistochemical staining and quantitative results demonstrated that the expression of these two

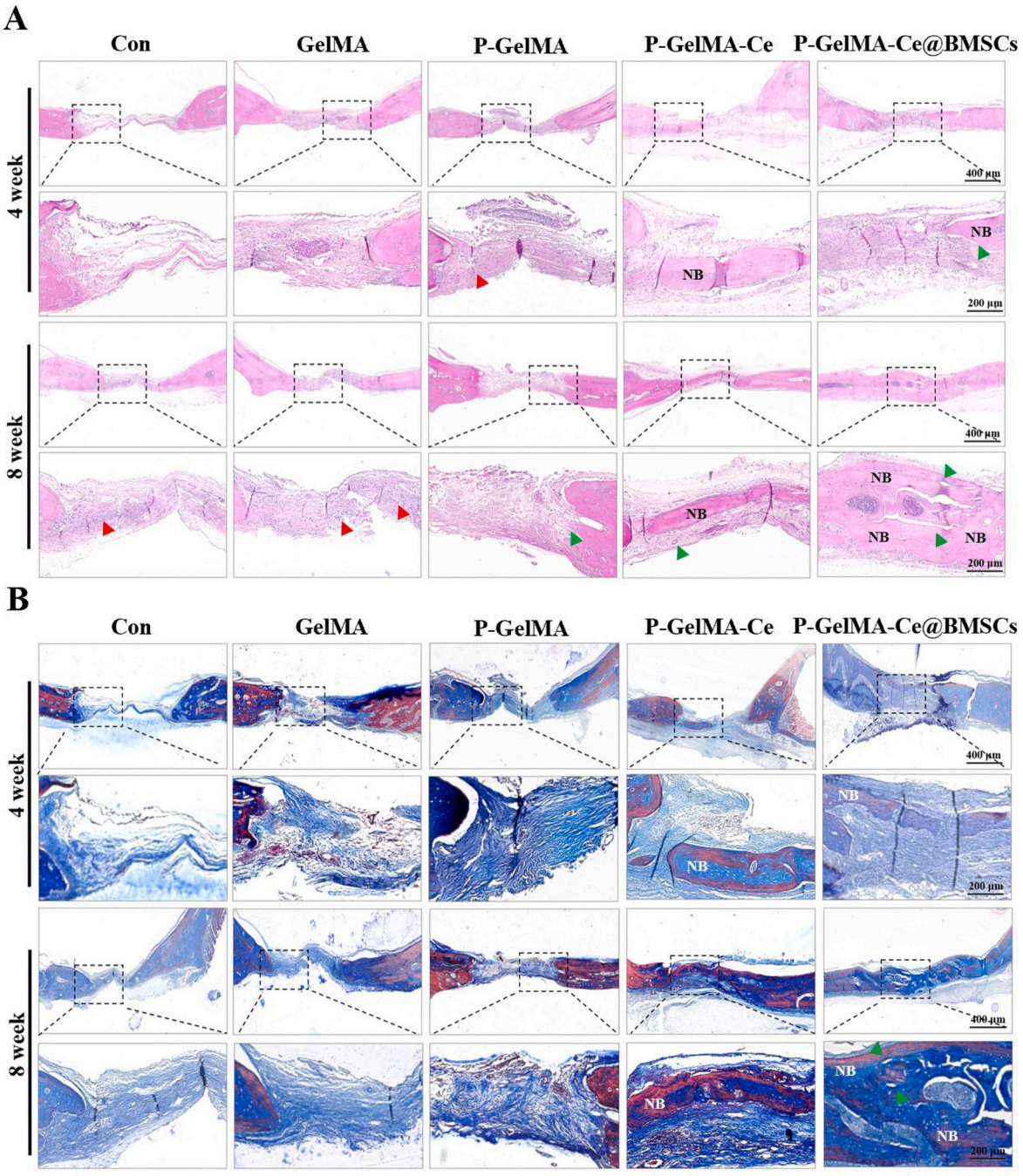


**Fig. 8.** Histological analysis of newly formed bone tissue after microspheres injection. (A) H&E and (B) Masson's trichrome staining of the critical-size cranial bone defect samples in the Con, GelMA, P-GelMA, and P-GelMA-Ce groups at 4 and 8 weeks. (NB: new bone, red arrow: osteoblasts, green arrow: blood vessels). (For interpretation of the references to color in this figure legend, the reader is referred to the Web version of this article.)

proteins in the P-GelMA-Ce group and P-GelMA-Ce@BMSCs group was substantially up-regulated compared to the P-GelMA group, particularly in the osteoblasts surrounding the new bone. Collagen I expression in the P-GelMA-Ce@BMSCs group increased by 21 % and 13 % compared to the P-GelMA-Ce group at 4 and 8 weeks, respectively. There was no statistically significant difference in the angiogenic marker protein VEGF between the P-GelMA-Ce group and P-GelMA-Ce@BMSCs group, with both reaching approximately 38 % and 50 % at the 4th and 8th weeks, respectively. In contrast, the expression levels of Collagen I and VEGF in the control, GelMA, and P-GelMA groups were lower, indicating limited bone regeneration capacity (Fig. 9A–D).

Paracrine signaling represents a crucial mechanism through which mesenchymal stem cells foster tissue regeneration.[31] Nevertheless, the paracrine activity of stem cells predominantly relies on the cell adhesion microenvironment [66]. In this investigation, P-GelMA-Ce hydrogel microspheres bolstered the paracrine activity of stem cells by offering a conducive microenvironment, both through physical protection and the promotion of cell adhesion and proliferation. Initially, hydrogel microspheres served to physically shield encapsulated cells from the shear forces generated during drug delivery through narrow needles [67]. Moreover, the use of hydrogel for cell transportation prevented the direct exposure of cells to harsh microenvironments detrimental to cellular metabolism. Consequently, hydrogel microspheres contributed to sustaining the paracrine capacity of transplanted cells by preserving cell viability. Furthermore, hydrogels that mimic the natural extracellular matrix (ECM) are beneficial to paracrine function by promoting cell adhesion, diffusion and proliferation [68]. In conclusion, the P-GelMA-Ce@BMSCs group appeared the most pronounced healing-promoting effect in boosting cranial defect repair.

## 4. Conclusions

In summary, a living and injectable porous hydrogel microsphere was developed for the regeneration of critical size bone defects. P-GelMA microspheres were prepared by microfluidic technology, then $Ce^{3+}$ was chelated on the surface of P-GelMA microspheres grafted with polyphosphate by coordination bonds, and finally incubated with exogenous BMSCs to construct novel live P-GelMA-Ce@BMSCs composite microspheres. With excellent cytocompatibility, the porous hydrogel microspheres could improve the survival and engraftment rates of stem cells by facilitating cell adhesion. In addition, when stimulated by $Ce^{3+}$ released from composite microspheres, BMSCs upregulated VEGF secretion and played a significant role in cerium-mediated vascularization and bone formation by accelerating cell-to-ECM and cell-to-cell interactions. Anyhow, the newly developed P-GelMA-Ce@BMSCs microspheres achieved a remarkable enhancement of physiochemical and biological properties, exhibiting extraordinary osteogenic and angiogenic activities in vitro and in vivo experiments.

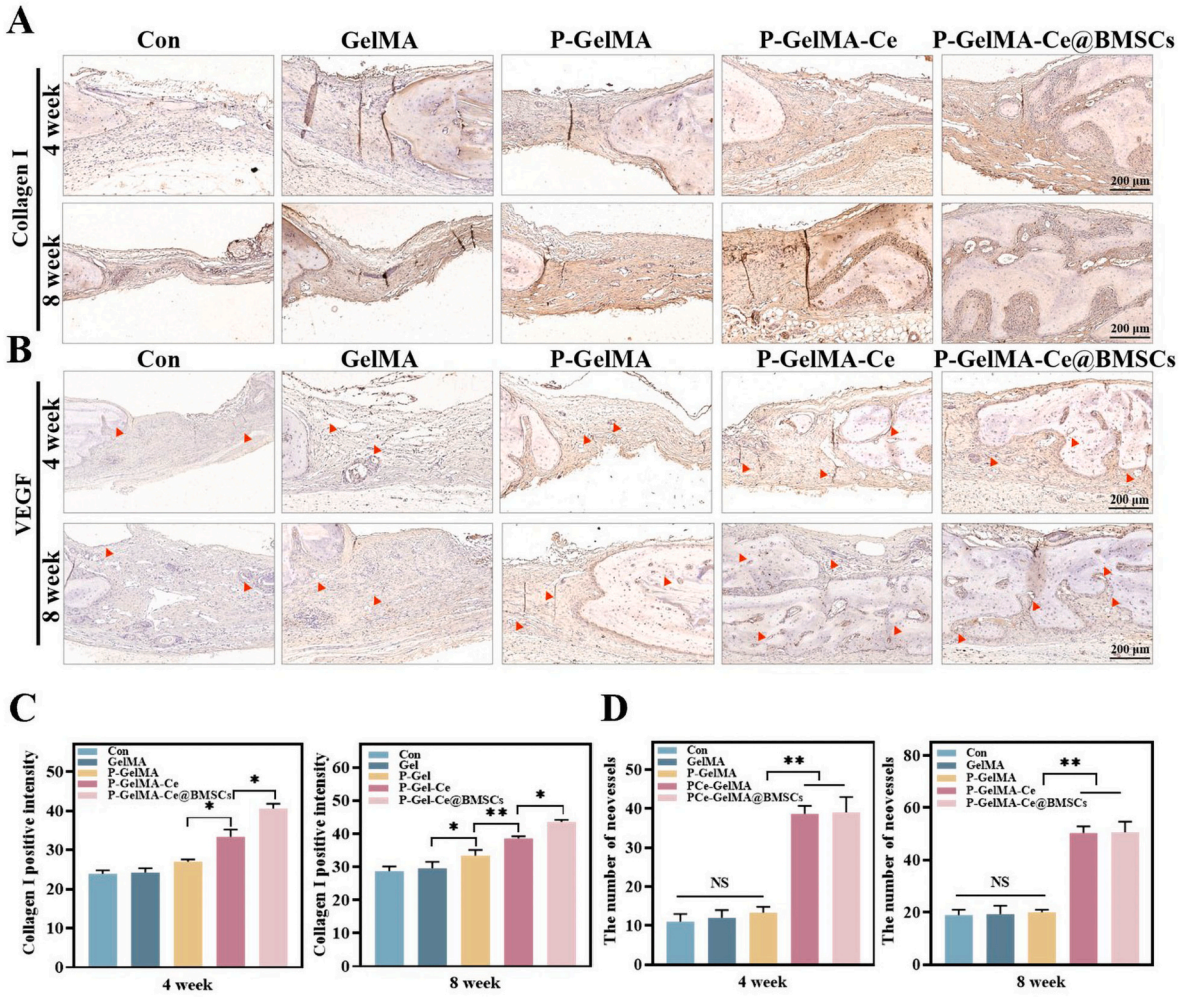


**Fig. 9.** Immunohistochemical staining of newly formed bone tissue after microspheres injection. (A, B) The immunohistochemical staining of Collagen I and VEGF in the Con, GelMA, P-GelMA, and P-GelMA-Ce groups after injection for 4 and 8 weeks. (red arrow: blood vessels). (C) Quantification of type I collagen positive intensity at 4 and 8 weeks. (D) Quantification of the number of new blood vessels at 4 and 8 weeks. (*, $P < 0.05$; **, $P < 0.01$). (For interpretation of the references to color in this figure legend, the reader is referred to the Web version of this article.)

We firmly believe that this kind of composite biologic scaffold based on metal ions will provide a promising therapeutic strategy for repairing clinical bone defects and provide inspiration for the development of BTE.

## Ethics approval and consent to participate

All animal experiments were approved by the Ethics Committee of the First Afliated Hospital of Soochow University.

## Consent for publication

All authors are consent for publication.

## Availability of data and materials

The data that support the findings of this study are available from the corresponding author upon reasonable request.

## Funding

This work was supported by grants from National Key R&D Program of China (Grant Nos: 2022YFC2502902), National Natural Science Foundation of China (Grant Nos: 82072442, 82272494, 82302664), Natural Science Foundation of Jiangsu Province (SBK2023043711), the Natural Science Foundation of Jiangsu Province (BK20230494), the Orthopaedic Medical Innovation Center of Jiangsu (CXZX202209), Key Laboratory of Orthopaedics of Suzhou (SZS2022017), the Priority Academic Program Development of Jiangsu Higher Education Institutions (PAPD), Gusu Innovation and Entrepreneur Leading Talents project (ZXL2023204).

## CRediT authorship contribution statement

**Junlin Liu:** Conceptualization, Data curation, Formal analysis, Investigation, Writing – original draft. **Zhangzhe Zhou:** Data curation, Formal analysis, Investigation, Project administration, Writing – original draft. **Mingzhuang Hou:** Data curation, Formal analysis, Investigation, Writing – original draft. **Xiaowei Xia:** Formal analysis, Investigation, Resources, Software, Supervision. **Yang Liu:** Investigation, Software. **Zhijian Zhao:** Software. **Yubin Wu:** Software. **Yaoge Deng:** Software. **Yijian Zhang:** Formal analysis, Resources, Software. **Fan He:** Conceptualization, Investigation, Project administration, Resources, Supervision, Writing – review & editing. **Yong Xu:** Conceptualization, Investigation, Project administration, Supervision, Writing – review & editing. **Xuesong Zhu:** Conceptualization, Project administration, Supervision, Writing – review & editing.

## Declaration of competing interest

The authors declare that they have no known competing financial interests or personal relationships that could have appeared to influence the work reported in this paper.

## Data availability

Data will be made available on request.

## Acknowledgments

Home for Researchers editorial team (www.home-for-researchers.com) is acknowledged for providing English language editing services.

## Appendix A. Supplementary data

Supplementary data to this article can be found online at https://doi.org/10.1016/j.mtbio.2024.100956.

## References

[1] J.S. Brown, C. Barry, M. Ho, R. Shaw, A new classification for mandibular defects after oncological resection, Lancet Oncol. 17 (2016) 23–30.
[2] J.E. Compston, M.R. McClung, W.D. Leslie, Osteoporosis, Lancet (London, England) 393 (10169) (2019) 364–376.
[3] J. Tuckermann, R.H. Adams, The endothelium-bone axis in development, homeostasis and bone and joint disease, Nat. Rev. Rheumatol. 17 (10) (2021) 608–620.
[4] A. Marrella, T.Y. Lee, D.H. Lee, S. Karuthedom, D. Syla, A. Chawla, A. Khademhosseini, H.L. Jang, Engineering vascularized and innervated bone biomaterials for improved skeletal tissue regeneration, Mater. Today 21 (4) (2018) 362–376.
[5] D. Holmes, Non-union bone fracture: a quicker fix, Nature 550 (7677) (2017) S193.
[6] B. Wildemann, A. Ignatius, F. Leung, L.A. Taitsman, R.M. Smith, R. Pesántez, M. J. Stoddart, R.G. Richards, J.B. Jupiter, Non-union bone fractures, Nat. Rev. Dis. Prim. 7 (1) (2021) 57.
[7] T. Später, M. Assunção, K.K. Lit, G. Gong, X. Wang, Y.Y. Chen, Y. Rao, Y. Li, C.H. K. Yiu, M.W. Laschke, M.D. Menger, D. Wang, R.S. Tuan, K.H. Khoo, M. Raghunath, J. Guo, A. Blocki, Engineering microparticles based on solidified stem cell secretome with an augmented pro-angiogenic factor portfolio for therapeutic angiogenesis, Bioact. Mater. 17 (2022) 526–541.
[8] L. Wu, Y. Gu, L. Liu, J. Tang, J. Mao, K. Xi, Z. Jiang, Y. Zhou, Y. Xu, L. Deng, L. Chen, W. Cui, Hierarchical micro/nanofibrous membranes of sustained releasing VEGF for periosteal regeneration, Biomaterials 227 (2020) 119555.
[9] H. Madry, L. Gao, A. Rey-Rico, J.K. Venkatesan, K. Müller-Brandt, X. Cai, L. Goebel, G. Schmitt, S. Speicher-Mentges, D. Zurakowski, M.D. Menger, M.W. Laschke, M. Cucchiarini, Thermosensitive hydrogel based on PEO-PPO-PEO poloxamers for a controlled in situ release of recombinant adeno-associated viral vectors for effective gene therapy of cartilage defects, Adv. Mater. 32 (2) (2020) e1906508.
[10] V. Mastrullo, W. Cathery, E. Velliou, P. Madeddu, P. Campagnolo, Angiogenesis in tissue engineering: as nature intended? Front. Bioeng. Biotechnol. 8 (2020) 188.
[11] Z. Wang, Z. Wang, W.W. Lu, W. Zhen, D. Yang, S.J.N.A.M. Peng, Novel biomaterial strategies for controlled growth factor delivery for biomedical applications, NPG Asia Mater. 9 (10) (2017) e435, e435.
[12] X. Ren, M. Zhao, B. Lash, M.M. Martino, Z. Julier, Growth factor engineering strategies for regenerative medicine applications, Front. Bioeng. Biotechnol. 7 (2019) 469.
[13] Y. Tang, M. Hu, Y. Xu, F. Chen, S. Chen, M. Chen, Y. Qi, M. Shen, C. Wang, Y. Lu, Z. Zhang, H. Zeng, Y. Quan, F. Wang, Y. Su, D. Zeng, S. Wang, J. Wang, Megakaryocytes promote bone formation through coupling osteogenesis with angiogenesis by secreting TGF-β1, Theranostics 10 (5) (2020) 2229–2242.
[14] J. Yan, J.W. Herzog, K. Tsang, C.A. Brennan, M.A. Bower, W.S. Garrett, B.R. Sartor, A.O. Aliprantis, J.F. Charles, Gut microbiota induce IGF-1 and promote bone formation and growth, Proc. Natl. Acad. Sci. U.S.A. 113 (47) (2016) E7554–e7563.
[15] E. Bosch-Rué, L. Diez-Tercero, B. Giordano-Kelhoffer, L.M. Delgado, B.M. Bosch, M. Hoyos-Nogués, M.A. Mateos-Timoneda, P.A. Tran, F.J. Gil, R.A. Perez, Biological roles and delivery strategies for ions to promote osteogenic induction, Front. Cell Dev. Biol. (2021) 1809.
[16] A. Hoppe, V. Mouriño, A.R. Boccaccini, Therapeutic inorganic ions in bioactive glasses to enhance bone formation and beyond, Biomater. Sci. 1 (3) (2013) 254–256.
[17] V. Mouriño, J.P. Cattalini, A.R. Boccaccini, Metallic ions as therapeutic agents in tissue engineering scaffolds: an overview of their biological applications and strategies for new developments, J. R. Soc., Interface 9 (68) (2012) 401–419.
[18] B. Zambelli, F. Musiani, S. Ciurli, Metal ion-mediated DNA-protein interactions, Metal ions in life sciences 10 (2012) 135–170.
[19] F. Elinder, P. Arhem, Metal ion effects on ion channel gating, Q. Rev. Biophys. 36 (4) (2003) 373–427.
[20] A.K. Vashishtha, J. Wang, W.H. Konigsberg, Different divalent cations alter the kinetics and fidelity of DNA polymerases, J. Biol. Chem. 291 (40) (2016) 20869–20875.
[21] È. Bosch-Rué, L. Díez-Tercero, J.O. Buitrago, E. Castro, R.A. Pérez, Angiogenic and immunomodulation role of ions for initial stages of bone tissue regeneration, Acta Biomater. 166 (2023) 14–41.
[22] E. O'Neill, G. Awale, L. Daneshmandi, O. Umerah, K.W. Lo, The roles of ions on bone regeneration, Drug Discov. Today 23 (4) (2018) 879–890.
[23] S. Zaichick, V. Zaichick, V. Karandashev, S. Nosenko, Accumulation of rare earth elements in human bone within the lifespan, Metallomics : integrated biometal science 3 (2) (2011) 186–194.
[24] X. Fang, H. Song, Synthesis of cerium oxide nanoparticles loaded on chitosan for enhanced auto-catalytic regenerative ability and biocompatibility for the spinal cord injury repair, J. Photochem. Photobiol. B Biol. 191 (2019) 83–87.
[25] A. Marino, C. Tonda-Turo, D. De Pasquale, F. Ruini, G. Genchi, S. Nitti, V. Cappello, M. Gemmi, V. Mattoli, G. Ciardelli, G. Ciofani, Gelatin/nanoceria nanocomposite fibers as antioxidant scaffolds for neuronal regeneration, Biochimica et biophysica acta, General subjects 1861 (2) (2017) 386–395.
[26] P. Zhao, H. Hu, J. Liu, Q. Ke, X. Peng, H. Ding, Y. Guo, Gadolinium phosphate/chitosan scaffolds promote new bone regeneration via Smad/Runx2 pathway, Chem. Eng. J. 359 (2019) 1120–1129.
[27] R. Leu Alexa, A. Cucuruz, C.-D. Ghițulică, G. Voicu, L.-R. Stamat, S. Dinescu, G. M. Vlasceanu, C. Stavarache, R. Ianchis, H. Iovu, M. Costache, 3D printable

composite biomaterials based on GelMA and hydroxyapatite powders doped with cerium ions for bone tissue regeneration, Int. J. Mol. Sci. 23 (3) (2022) 1841.
[28] A. Zambon, G. Malavasi, A. Pallini, F. Fraulini, G. Lusvardi, Cerium containing bioactive glasses: a review, ACS Biomater. Sci. Eng. 7 (9) (2021) 4388–4401.
[29] R.M. Hernández, G. Orive, A. Murua, J.L. Pedraz, Microcapsules and microcarriers for in situ cell delivery, Adv. Drug Deliv. Rev. 62 (7–8) (2010) 711–730.
[30] L. Shang, Y. Cheng, Y. Zhao, Emerging droplet microfluidics, Chem. Rev. 117 (12) (2017) 7964–8040.
[31] X. Li, X. Li, J. Yang, J. Lin, Y. Zhu, X. Xu, W. Cui, Living and injectable porous hydrogel microsphere with paracrine activity for cartilage regeneration, Small 19 (17) (2023) e2207211.
[32] V.T. Tran, J.P. Benoît, M.C. Venier-Julienne, Why and how to prepare biodegradable, monodispersed, polymeric microparticles in the field of pharmacy? Int. J. Pharm. 407 (1–2) (2011) 1–11.
[33] J.J.M.C. Thiele, Physics, polymer material design by microfluidics inspired by cell biology and cell-free biotechnology, Macromol. Chem. Phys. 218 (2) (2017) 1600429.
[34] W.J. Duncanson, T. Lin, A.R. Abate, S. Seiffert, R.K. Shah, D.A. Weitz, Microfluidic synthesis of advanced microparticles for encapsulation and controlled release, Lab Chip. 12 (12) (2012) 2135–2145.
[35] T.S. Shim, S.H. Kim, S.M.J.P. Yang, P.S. Characterization, Elaborate design strategies toward novel microcarriers for controlled encapsulation and release, Part. Part. Syst. Char. 30 (1) (2013) 9–45.
[36] W. Li, L. Zhang, X. Ge, B. Xu, W. Zhang, L. Qu, C.-H. Choi, J. Xu, A. Zhang, H.J.C.S. R. Lee, Microfluidic fabrication of microparticles for biomedical applications, Chem. Soc. Rev. 47 (15) (2018) 5646–5683.
[37] D. Zheng, W. Chen, H. Ruan, Z. Cai, X. Chen, T. Chen, Y. Zhang, W. Cui, H. Chen, H. Shen, Metformin-hydrogel with glucose responsiveness for chronic inflammatory suppression, Eng. J. 428 (2022) 131064.
[38] L. Xu, S. Gao, R. Zhou, F. Zhou, Y. Qiao, D. Qiu, Bioactive pore-forming bone adhesives facilitating cell ingrowth for fracture healing, Adv. Mater. 32 (2020) 1907491.
[39] X. Wang, J. Fang, W. Zhu, C. Zhong, D. Ye, M. Zhu, X. Lu, Y. Zhao, F. Ren, Bioinspired highly anisotropic, ultrastrong and stiff, and osteoconductive mineralized wood hydrogel composites for bone repair, Adv. Funct. Mater. 31 (2021) 2010068.
[40] J. Lu, F. Yang, Q. Ke, X. Xie, Y. Guo, Magnetic nanoparticles modified-porous scaffolds for bone regeneration and photothermal therapy against tumors, Nanomed-Nanotechnol 14 (2018) 811–822.
[41] N. Huebsch, E. Lippens, K. Lee, M. Mehta, S.T. Koshy, M.C. Darnell, R.M. Desai, C. M. Madl, M. Xu, X. Zhao, O. Chaudhuri, C. Verbeke, W.S. Kim, K. Alim, A. Mammoto, D.E. Ingber, G.N. Duda, D.J. Mooney, Matrix elasticity of void-forming hydrogels controls transplanted-stem-cell-mediated bone formation, Nat. Mater. 14 (14) (2015) 1269–1277.
[42] F. Zhao, W. Xie, W. Zhang, X. Fu, W. Gao, B. Lei, X. Chen, 3D printing nanoscale bioactive glass scaffolds enhance osteoblast migration and extramembranous osteogenesis through stimulating immunomodulation, Adv. Healthcare Mater. 7 (2018) 1800361.
[43] S. Zaichick, V. Zaichick, V. Karandashev, S. Nosenko, Accumulation of rare earth elements in human bone within the lifespan, Metallomics 3 (2011) 186–194.
[44] E. O'Neill, G. Awale, L. Daneshmandi, O. Umerah, K.W. Lo, The roles of ions on bone regeneration, Drug Discov. Today 23 (2018) 879–890.
[45] Q. Wan, K. Jiao, Y. Ma, B. Gao, Z. Mu, Y. Wang, L. Duan, K. Xu, J. Gu, J. Yan, J. Li, M. Shen, F. Tay, L. Niu, Smart, biomimetic periosteum created from the cerium (III, IV) oxide-mineralized eggshell membrane, ACS Appl. Mater. Interfaces 14 (2022) 14103–14119.
[46] J. Li, J. Wen, B. Li, W. Li, W. Qiao, J. Shen, W. Jin, X. Jiang, K.W.K. Yeung, P. Chu, Valence state manipulation of cerium oxide nanoparticles on a titanium surface for modulating cell fate and bone formation, Adv. Sci. 18 (2017) 1700678.
[47] X. Zhao, S. Liu, L. Yildirimer, H. Zhao, R. Ding, H. Wang, W. Cui, D. Weitz, Microfluidics-Assisted osteogenesis: injectable stem cell-laden photocrosslinkable microspheres fabricated using microfluidics for rapid generation of osteogenic tissue constructs, Adv. Funct. Mater. 26 (2016) 2809.
[48] T.E. Paterson, G. Gigliobianco, C. Sherborne, N.H. Green, J.M. Dugan, S. MacNeil, G.C. Reilly, F. Claeyssens, Porous microspheres support mesenchymal progenitor cell ingrowth and stimulate angiogenesis, APL Bioeng. 26 (2018) 026103.
[49] Y. Lei, Y. Wang, J. Shen, Z. Cai, Y. Zeng, P. Zhao, J. Liao, C. Lian, N. Hu, X. Luo, W. Cui, W. Huang, Stem cell-recruiting injectable microgels for repairing osteoarthritis, Adv. Funct. Mater. 31 (2021) 2105084.
[50] Y. Huang, M. Zhang, M. Jin, T. Ma, J. Guo, X. Zhai, Y. Du, Recent advances on cerium oxide-based biomaterials: toward the next generation of intelligent theranostics platforms, Adv. Healthcare Mater. 12 (25) (2023) e2300748.
[51] B. Lu, D. Zhu, J. Yin, H. Xu, C. Zhang, Q. Ke, Y. Gao, Y. Guo, Incorporation of cerium oxide in hollow mesoporous bioglass scaffolds for enhanced bone regeneration by activating the ERK signaling pathway, Biofabrication 11 (2019) 025012.
[52] A. Kuźnik, A. Październiok-Holewa, P. Jewula, N. Kuźnik, Bisphosphonates-much more than only drugs for bone diseases, Eur. J. Pharmacol. 866 (2020) 172773.
[53] F. Diomede, G.D. Marconi, L. Fonticoli, J. Pizzicanella, I. Merciaro, P. Bramanti, E. Mazzon, O. Trubiani, Functional relationship between osteogenesis and angiogenesis in tissue regeneration, Int. J. Mol. Sci. 21 (2020) 3242.
[54] J. Cui, X. Yu, B. Yu, X. Yang, Z. Fu, J. Wan, M. Zhu, X. Wang, K. Lin, Coaxially fabricated dual-drug loading electrospinning fibrous mat with programmed releasing behavior to boost vascularized bone regeneration, Adv. Healthcare Mater. 11 (2022) 2200571.
[55] M. Yin, J. Wu, M. Deng, P. Wang, G. Ji, M. Wang, N.T. Blum, W. Zhang, H. Shi, N. Jia, X. Wang, P. Huang, Multifunctional magnesium organic framework-based microneedle patch for accelerating diabetic wound healing, ACS Nano 15 (2021) 17842–17853.
[56] Y. Wang, Z. Cao, Q. Wei, K. Ma, W. Hu, W, Q. Huang, J. Su, H. Li, C. Zhang, X. Fu, VH298-loaded extracellular vesicles released from gelatin methacryloyl hydrogel facilitate diabetic wound healing by HIF-1α-mediated enhancement of angiogenesis, Acta Biomater. 147 (2022) 342–355.
[57] Q. Bai, K. Han, K. Dong, C. Zheng, Y. Zhang, Q. Long, T. Lu, Potential applications of nanomaterials and technology for diabetic wound healing, Int. J. Nanomed. 15 (2020) 9717–9743.
[58] T. Asahara, T. Murohara, A. Sullivan, M. Silver, R. Zee, T. Li, B. Witzenbichler, G. Schatteman, J.M. Isner, Isolation of putative progenitor endothelial cells for angiogenesis, Science 275 (1997) 964–967.
[59] A. Bronckaers, P. Hilkens, W. Martens, P. Gervois, J. Ratajczak, T. Struys, I. Lambrichts, Mesenchymal stem/stromal cells as a pharmacological and therapeutic approach to accelerate angiogenesis, Pharmacol. Ther. 143 (143) (2014) 181–196.
[60] C. Dou, J. Li, J. He, F. Luo, T. Yu, Q. Dai, Y. Chen, J. Xu, X. Yang, S. Dong, Bone-targeted pH-responsive cerium nanoparticles for anabolic therapy in osteoporosis, Bioact. Mater. 6 (2021) 4697–4706.
[61] J. Luo, S. Zhu, S. Tong, Y. Zhang, Y. Li, L. Cao, M. Kong, M. Luo, Q. Bi, Q. Zhang, Cerium oxide nanoparticles promote osteoplastic precursor differentiation by activating the Wnt pathway, Biol. Trace Elem. Res. 201 (2023) 865–873.
[62] C.M. Karner, F. Long, Wnt signaling and cellular metabolism in osteoblasts, Cell. Mol. Life Sci. 74 (2017) 1649–1657.
[63] Z. Zhang, F. Nör, M. Oh, C. Cucco, S. Shi, J.E. Nör, Wnt/β-Catenin signaling determines the vasculogenic fate of postnatal mesenchymal stem cells, Stem Cell. 34 (2016) 1576–1587.
[64] C.M. Sturgeon, A. Ditadi, G. Awong, M. Kennedy, G. Keller, Wnt signaling controls the specification of definitive and primitive hematopoiesis from human pluripotent stem cells, Nat. Biotechnol. 32 (2014) 554–561.
[65] K. Maeda, Y. Kobayashi, M. Koide, S. Uehara, M. Okamoto, A. Ishihara, T. Kayama, M. Saito, K. Marumo, The regulation of bone metabolism and disorders by Wnt signaling, Int. J. Mol. Sci. 20 (2019) 5525.
[66] J. Song, X. Lin, L. Ee, S. Li, M. Huang, A review on electrospinning as versatile supports for diverse nanofibers and their applications in environmental sensing, Adv Fiber Mater 5 (2023) 429–460.
[67] F. Hached, C. Vinatier, C. Le Visage, H. Gondé, J. Guicheux, G. Grimandi, Billon-Chabaud A. Biomaterial-assisted cell therapy in osteoarthritis: from mesenchymal stem cells to cell encapsulation, Best Pract. Res. Clin. Rheumatol. 31 (2017) 730–745.
[68] Y. Piao, H. You, T. Xu, H.P. Bei, I.Z. Piwko, Y.Y. Kwan, X. Zhao, XBiomedical applications of gelatin metgacryloyl hydrogels, Eng. Regener. 2 (2021) 47.